Corso di Laurea Magistrale in Ingegneria Aerospaziale

Tesi di Laurea Magistrale

Optimisation of sequences for space debris removal

Relatore:
Prof. Lorenzo Casalino

Candidato:
Raul Michelini

Luglio 2021

Alla mia famiglia, in particolar modo a mio fratello Igor
Per aver sempre creduto in me
Più di quanto potessi farlo io

A Simone
Partito insieme a me per questo viaggio
Diventato nel tempo un mentore e fratello

A Federico, Edoardo, Sofia e Giuseppe
Che pur conoscendo da poco tempo
Sono diventati gli amici sui quali so di poter sempre contare

A Simone C. e Maxime
Che pur essendo lontani
Mi sono sempre stati accanto

A Ludovica
Che ha saputo prendermi con pregi e difetti
Sostenendomi sempre in ciò che conta

Agli amici di Torino
Vi auguro di incontrare e conoscere persone come io ho trovato voi

A tutti gli amici di Vissandone

A tutti coloro che in qualche modo mi hanno accompagnato lungo questo cammino

Grazie.

Abstract

The gradual increase in space missions brings with it not only countless benefits for humanity but also several problems that cannot be ignored nowadays. The most relevant issue is the constant increase in space debris. These, also commonly called *space junk*, include: non-functional satellites, mission remnants such as abandoned launch vehicle stages and fragments of various types, which orbit the earth and represent a real risk to new space missions.
This issue has led space agencies to define different solutions to mitigate both the risk of orbital accidents and the increase of space debris, thus decreasing the probability of collisions. These solutions are: extending the operational life of satellites with a consequent reduction in the number of launches, design the satellite for end-of-life deorbiting, and the active removal of already orbiting debris.
In particular, this thesis focuses on the latter solution, analyzing and comparing two mission strategies for space debris removal through deorbiting via chemical propulsion.
The mission focuses on the removal of four debris generated by the Russian 'Kosmos 3M' launchers, which during their operational phase produced two clusters of debris at orbital inclinations of 74° (120 debris) and 82° (155 debris). The case studied foresees that the spacecraft is already on the first debris, on which the spacecraft waits for the time necessary to apply the deorbiting kit and then makes a transfer to the next debris. This operation is repeated until the arrival on the fourth debris, where the mission is considered to be concluded.
This thesis aims at optimizing the transfers between debris by minimizing propellant consumption. In order to do that, the most efficient of the two following strategies are applied: (i) the first consists in performing the transfer if the condition of orbit coplanarity is verified in a predefined time span; (ii) the second strategy, instead, is applied in the case in which the condition of coplanarity is not verified in the predefined time. The first strategy is performed using a single impulse, while the second one, since the orbits are non-coplanar, requires two impulses. The second strategy exists since the coplanarity condition may not be reached in a short period. Therefore, the objective is to optimize the mission, both in terms of mission time and ΔV (change in velocity) cost. Furthermore, a simplified formulation is applied, thus obtaining a computationally efficient algorithm.
The results obtained are compared with those obtained from applying other possible strategies and those derived from the non-simplified formulation. The purpose is to verify the validity of the proposed approach.

Sommario

L'aumento progressivo delle missioni spaziali porta con sè oltre che innumerevoli vantaggi per l'umanità, anche alcune problematiche che al giorno d'oggi non possono essere ignorate. La problematica più rilevante è il costante aumento di detriti spaziali, anche comunemente chiamati *rifiuti spaziali*, e includono: satelliti in disuso, resti di missione come stadi dei veicoli di lancio abbandonati e frammenti di vario tipo, che orbitando attorno alla terra rappresentano un rischio concreto per le nuove missioni spaziali. Tale problematica ha portato le agenzie spaziali a definire diverse soluzioni per mitigare sia il rischio di collisioni e incidenti orbitali, sia l'aumento dei detriti spaziali stessi. Queste soluzioni possono mirare a: prolungamento della vita operativa dei satelliti con la conseguente diminuzione del numero di lanci, la predisposizione in fase progettuale di una fase di deorbiting alla conclusione della vita operativa del satellite, e la rimozione fisica dei detriti già presenti in orbita.

In particolare, l'attenzione viene posta sull'ultima soluzione elencata analizzando e confrontando due strategie di missione atte alla rimozione di detriti spaziali tramite deorbiting mediante propulsione chimica.

La missione trattata prevede la rimozione di quattro detriti tra quelli generati dai lanciatori russi 'Kosmos 3M' che in fase operativa hanno prodotto due raggruppamenti di detriti alle inclinazioni orbitali di 74° (120 detriti) e 82° (155 detriti). Il caso studiato prevede che il veicolo spaziale si trovi già sul primo detrito, sul quale viene atteso il tempo necessario per l'applicazione del kit di deorbiting, per poi compiere una trasferta al detrito successivo. Questa operazione viene ripetuta fino all'arrivo sul quarto detrito, dove la missione si considera conclusa.

Questa tesi mira all'ottimizzazione dei trasferimenti tra un detrito e l'altro minimizzando il consumo di propellente. Ciò avviene applicando la più efficiente tra le seguenti strategie: (i) la prima strategia consiste nell'attuare il trasferimento se in un arco di tempo prestabilito si verificherà la condizione di complanarità tra le orbite; (ii) la seconda strategia, invece, viene applicata nel caso in cui nel tempo prestabilito la condizione di complanarità non viene verificata. Quest'ultima strategia viene considerata in quanto il verificarsi della condizione di complanarità potrebbe richiedere tempi eccessivamente lunghi. Si precisa che l'ottimizzazione della missione di rimozione è trattata sia dal punto di vista del tempo, sia dal punto di vista del costo in termini di ΔV (impulso in velocità) utilizzando al tempo stesso un algoritmo che sia efficiente anche dal punto di vista computazionale, mediante l'applicazione di una formulazione semplificata.

I risultati ottenuti vengono confrontati con quelli ricavati dall'applicazione di altre possibili strategie e con quelli derivati dalla formulazione non semplificata, l'intento è quello di verificare la validità dell'approccio proposto.

Contents

List of Figures

List of Tables

Chapter 1

Introduction

The steady increase of debris in space surrounding the Earth brings with it the need to remove some of it, in order to avoid a future without further launches due to the danger of collisions and accidents in space. Since a mission to remove one debris at a time would be too costly, the thesis aims to develop a mission that includes the sequential removal of four space debris. Since debris is grouped in certain bands according to its origin, this sequence can be combined according to mission requirements and constraints, and the purpose is to optimise this sequence so that is cost-effective and the transfers from one debris to the next are optimal. The mission is therefore as follows: departure from the first debris where one waits a service time necessary for the application of the de-orbiting kit, transfer to the second debris via chemical propulsion with the possibility of using two different strategies, arrival at the second debris and so on until the fourth debris. Upon arrival at the fourth debris, the mission is considered to be completed. A series of possible mission scenarios that are efficient will then be obtained. The mathematical model is a simplified model, so the results will not be precise but quite reliable and less expensive from a computational point of view. The applied model is part of the Simplified General Perturbation models (SGP) and introduces the following simplifications: semi-major axis, eccentricity and orbital inclination are assumed constant; gravitational forces of other celestial bodies and radiation are neglected since we are in Low Earth Orbit (LEO); atmospheric resistance is not considered and the only orbital perturbation taken into account is that resulting from the Earth's oblateness.

1.1 Thesis Outline

After this brief introduction, section 2 summarises the evolution of space debris from its inception to the present day, describes the main collisions over the years, discusses the Kessler syndrome and explains how debris is classified and catalogued. It then describes the main space debris removal methods that are being considered today.

Section 3 contains the derivation of the complete model, starting from the basis of orbital mechanics, deriving orbital elements and Kepler's laws of planetary motion and then introducing orbital perturbations and explaining how these perturb the motion of orbiting bodies. Section 3.3 describes the transfer manoeuvres, in particular, the Hohmann transfer orbit and how this manoeuvre can be adapted for the mission at hand. At the end of this section, a brief description of the mass budget of the mission.

Section 4 is focused on the description of the mission. After a general introduction, in section 4.2.1 and 4.2.2 is explained more precisely what happens during transfers in case one or the other strategy is used. Follows 4.3 where the de-orbiting technique used for the mission is briefly described.

Section 5 is dedicated to the explanations of the results obtained from the calculations. In the first part, section 5.1, are described all data given in input to the code to obtain results. After a brief explanation of the original code, results follow.

Finally, section 6 contains some concluding remarks and some possible future developments of this work.

Chapter 2

Space Debris

The era of artificial satellites began on 4 October 1957 with the launch of Sputnik I (a probe about the size of a football), put into orbit by the Soviet Union.

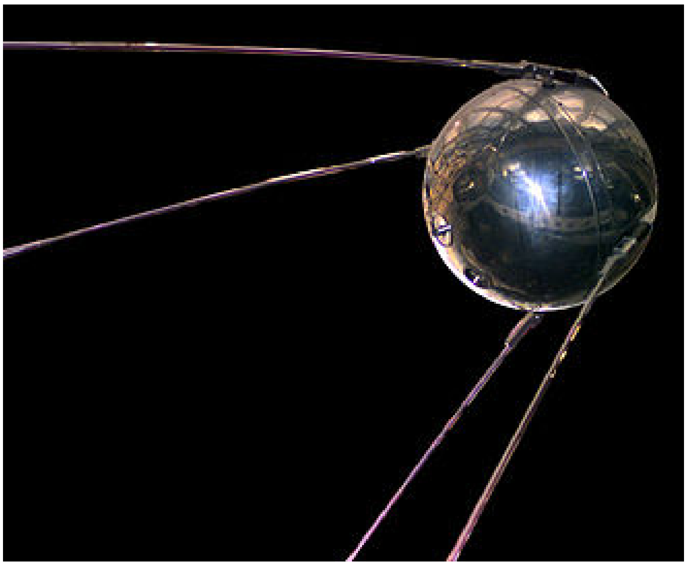

Figure 2.1: First artificial satellite Sputnik I.

On 1 January 1958, Sputnik I reentered the Earth's atmosphere. After this first launch, the Soviet Union and the United States of America started an informal competition called *Space race* intending to conquer space. In fact, about four months after the launch of Sputnik I, on 31 January 1958, the United States launched its first satellite, Explorer I. Interest in space technology then spread to an ever-increasing number of nations, gradually increasing the number of artificial satellites orbiting around the Earth. Significant historical achievements include the following events: 12 April 1961, Yuri Gagarin, the first man to fly into space. In August 1964, the first geostationary satellite, 15 December 1965, the first orbital rendezvous, and less than a year later there was a docking manoeuvre, 1969, Yuri Gagarin, the first man on the moon, then in 1971 the first space station (Salyut 1), the first space probe to orbit Mars. On 15 July 1975, the first international US-USSR mission (Apollo-Sojuz) took place, where the Sojuz 19 docked with the Apollo capsule, allowing the two crews to interact with each other. The satellites that were launched had various purposes, e.g. telecommunications, meteorological, astronomy research and spy satellites.

It can be therefore distinguished:

- Scientific satellite: for pure research in astronomy or geophysics, such as the Hubble Space Telescope.
- Application satellite: used for military or civilian purposes. These can be subdivided into:
  - Telecommunications satellites.
  - Meteorological satellites (*METEOSAT*).
  - Satellites built for remote sensing, mapping and observation of Earth's surface (*Landsat*).
  - Navigation satellites (*GPS*).
  - Militar satellites.
  - Orbiting stations(*ISS*).

During all these years and the years that followed, thousands of satellites were launched, and orbits began to be populated, first in the low orbits defined as *Low Earth Orbit* (LEO), which lie between the Earth's atmosphere and the Van Allen belts (between 160 km and 2000 km), and later in the orbits defined as *Medium Earth Orbit* (MEO), located between 2000 km and 36000 km, and in the *Geostationary Orbit* (GEO), which are placed at about 36000 km, so that the revolution period of the satellite coincides with the rotation period of the Earth.

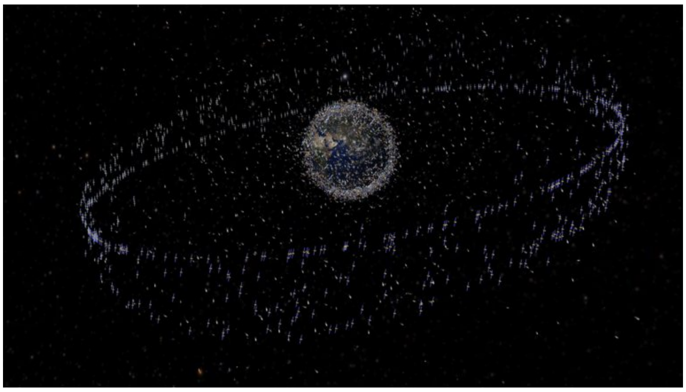

Figure 2.2: Debris population.

As can be imagined, not all launches were successful, and as the number of launches increased, so did the probability of accidents. In fact, just four years after the launch of Sputnik 1, the first in-orbit explosion occurred, when an American launcher exploded shortly after releasing the payload, generating about 300 fragments. There were also deliberate explosions (against spy satellites, for example).

Various types of collisions and accidents have occurred over the years, so the number of fragments increased, making it necessary to classify, track and dispose what is known as *space debris*.

As described in [1], the collisions that have occurred can be distinguished:

- Intentional collisions intended to destroy satellites through the use of anti-satellite weapons:
  - The Soviet Union, during the 1970-80s, with its 'Istrebitel Sputnikov' programme, conducted several tests for their interceptor satellite and destroyed target satellites created specifically for the purpose of the test (IS-P/I2M).
  - In 1985, the US destroyed the 'Solwind P78-1', an orbiting solar observatory, during a counter-satellite missile test.
  - In january 2007, the destruction of the meteorological satellite 'Fengyun FY-1C', during a Chinese anti-satellite test.[2]
  - In 2008, during operation 'Burn Frost', a non-functioning U.S. reconnaissance satellite (USA-193) was intercepted and destroyed.
- Unintentional low-speed collisions during rendezvous operations and docking manoeuvres:

  - In 1994, the collision between 'Soyuz TM 17' and Russian space station 'Mir'.
  - In 1997, the collision between the 'Progress M 34' spacecraft and the Russian space station 'Mir' during manual docking.
  - In 2005, collision during an orbital rendezvous manoeuvre, between 'USA DART' spacecraft and communication satellite 'USA MUBLCOM'.

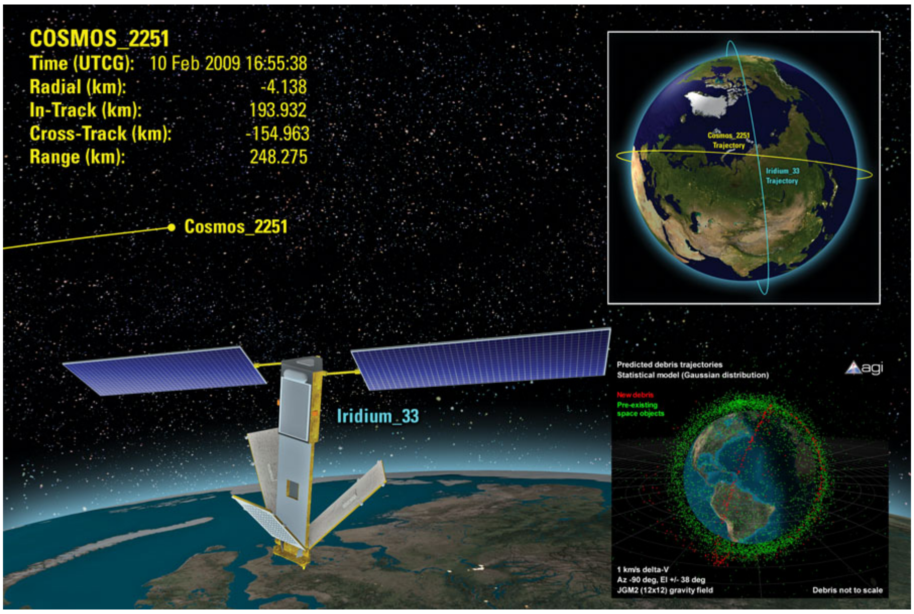

Figure 2.3: Collision between 'Iridium-33' and 'Cosmos-2251'.

- High-speed collisions between active satellites and orbiting debris:
  - In 1996, the collision between the French reconnaissance satellite 'Cerise' and debris produced by an 'Ariane' rocket.
  - The collision between the 'Iridium 33' communication satellite and the Russian 'Cosmos 2251' communication satellite in February 2009, resulting in the destruction of both satellites (Figure 2.3).[3]
  - On 22 January 2013, the collision between debris coming from Chinese 'Fengyun 1C' and the Russian nano-satellite 'Blits' changing both its orbit and rotation rate. [2][4]
  - On 22 May 2013, the collision between two CubeSats, Ecuador's 'NEE 01 Pegaso' and Argentina's 'CubeBug 1', forming a cloud of debris.

Table 2.1 lists the main space debris producing events, including the explosion of upper stages and satellite collisions:[5]

Common Name	Year	Altitude [km]	Catalogued debris	Debris in orbit	Assessed cause of breakup
Fengyun-1C	2007	850	3428	2880	Intentional collision
Cosmos 2251	2009	790	1668	1141	Accidental collision
STEP-2 Rocket Body	1996	625	754	84	Accidental explosion
Iridium 33	2009	790	628	364	Accidental collision
Cosmos 2421	2008	410	509	0	Unknown
SPOT-1 Rocket Body	1986	805	498	32	Accidental explosion
OV2-1 / LCS 2 Rocket Body	1965	740	473	33	Accidental explosion
CBERS 1 / SACI 1 Rocket Body	2000	740	431	210	Accidental explosion
Nimbus 4 Rocket Body	1970	1075	376	235	Accidental explosion
TES Rocket Body	2001	670	372	80	Accidental explosion

Table 2.1: Top 10 breakups, January 2016

2.1 Definition of Space Debris

Space debris (also known as *space junk*) is a term for defunct human-made objects in space, principally in Earth orbit, which no longer serves a useful function. These include derelict spacecraft, nonfunctional spacecraft, abandoned launch vehicle stages, mission-related debris and fragmentation debris from the breakup of derelict rocket bodies and spacecraft.[6]

Man-made objects in Earth orbit can be divided into the following categories:

- Breakup debris (fragmentations).
- Payloads/spacecrafts, grouping operational satellites and vehicles.
- Mission-related debris, i.e. all objects released intentionally.
- Rocket bodies, grouping upper stages, empty tanks and launcher fairings.
- Anomalous debris, comprising all that does not fall into the other categories.

The percentage distribution of the listed objects is shown in figure 2.4 :[1]

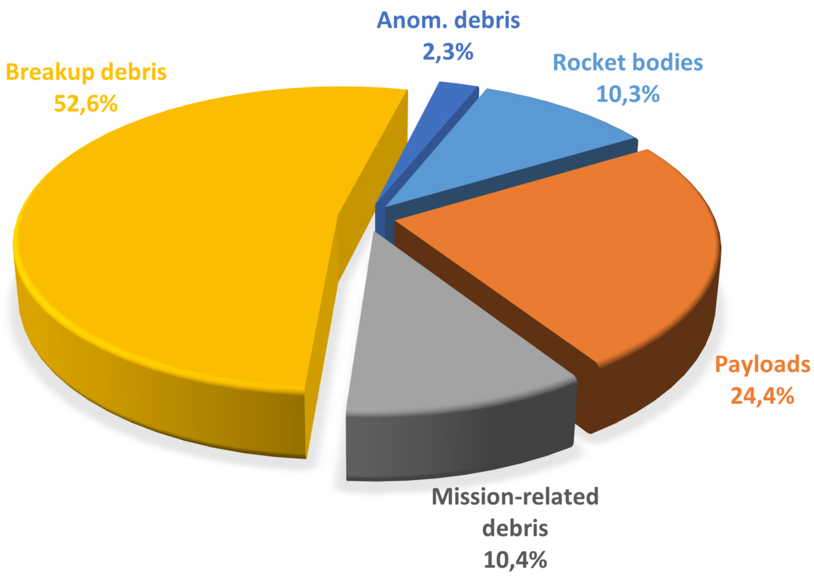

Figure 2.4: Relative segments of the cataloged in-orbit Earth satellite population.

The most important category is break up debris, as is evident from the graph, as this includes many kinds of breakups, it can be further divided into subcategories:[1]

- Deliberate actions.
- Propulsion-related breakups include malfunctions during orbital injection or manoeuvres, subsequent explosions based on residual propellants and failures of active attitude control system.[7]
- Accidental collisions.
- Battery.
- Unknown, includes all cases for which it cannot be proved that it belongs to a specific category.

In Figure 2.5 it can be seen divided into percentages:

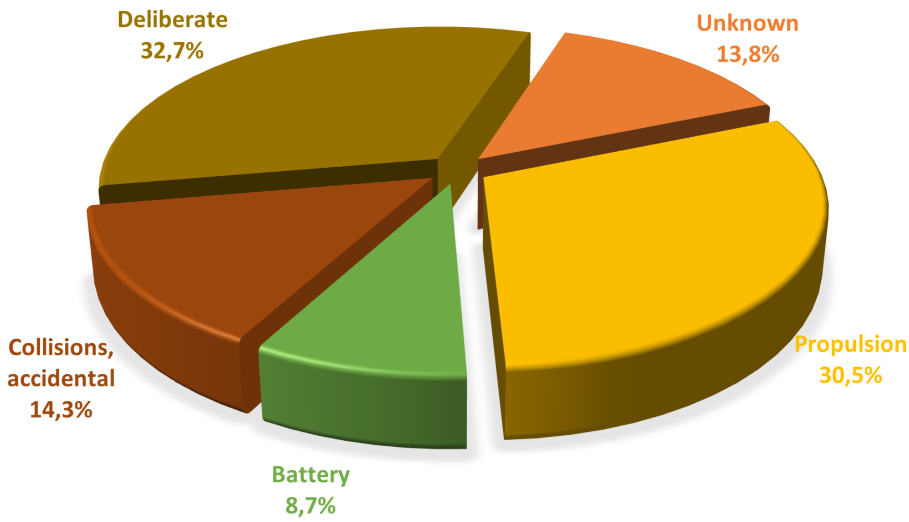

Figure 2.5: Proportion of cataloged satellite breakup debris.

It is noted that the percentage concerning deliberate actions, often associated with activities related to national security, was formerly the most frequently occurring class. However, only one such event occurred during the decade from 1997 until the 'Fengyun 1C' event in January 2007. On average, the resulting debris from deliberate actions are short-lived, the exception being 'Fengyun 1C'. Rocket body events are carried as Unknown until a failure mechanism can be confidently identified for that rocket body design and is associated with a given rocket body event.[1]

2.1.1 Kessler Syndrome

Large objects such as inactive satellites or upper stages are the main source of debris generation due to their mass and higher probability of being involved in a collision: a single collision event can result in a huge amount of debris.
Graph 2.9 shows the trend in debris generation over the years:[8]

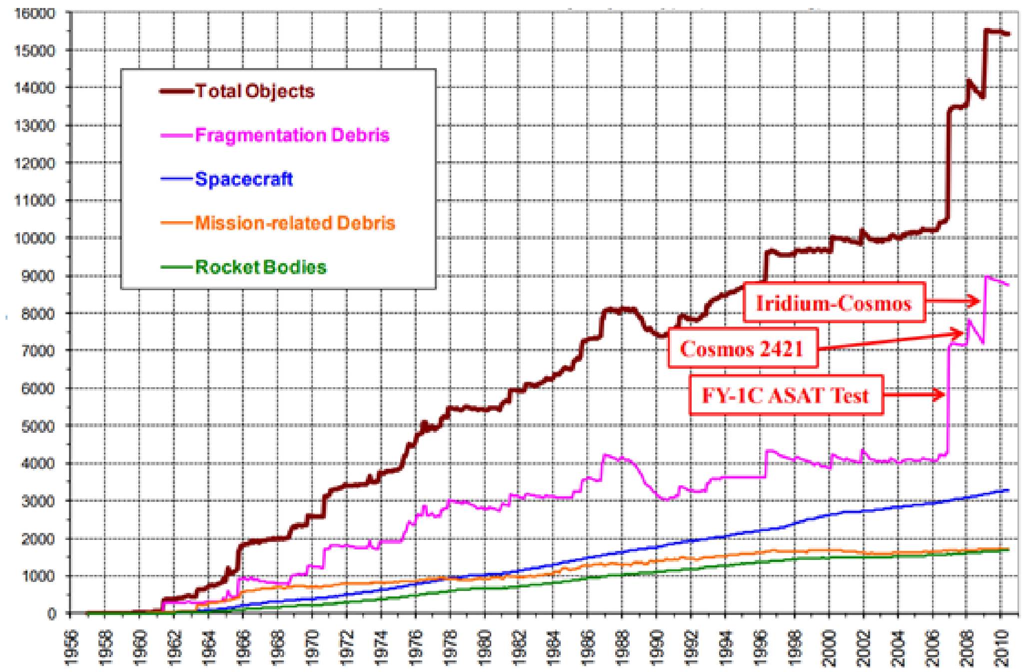

Figure 2.6: Number of Objects in Earth Orbit by Object Type (SSN Catalog).

As it might be seen from the graph 2.9, constant growth of debris is evident since any artificial object launched into space was usually abandoned at the end of its operational life.

Kessler, in 1978, predicted a possible scenario for the 2000s where space would no longer be usable for a long time due to the density of space debris caused by launches, which would lead to an increasing number of collisions, thus creating a chain reaction with an exponential increase in space debris and the risk of further collisions. This effect is now known as *Kessler syndrome*.[9]

Immediately after its publication, this problem was not considered, but it happened a few years later, in the 1980s when satellites were already being designed for atmospheric re-entry at the end of their operational life. These new measures were not always adopted because of cost and time issues - it was still the cold war period. Debris in space continued to increase even though this problem was known.

In figure 2.7 can be seen a graph that represents Spatial density (objects per unit volume). It is the effective number of spacecraft and other objects as a function of altitude. Effective number, rather than the simple counting of objects, is used because many objects traverse the altitude regions of interest yet contribute little to the local collision hazard.

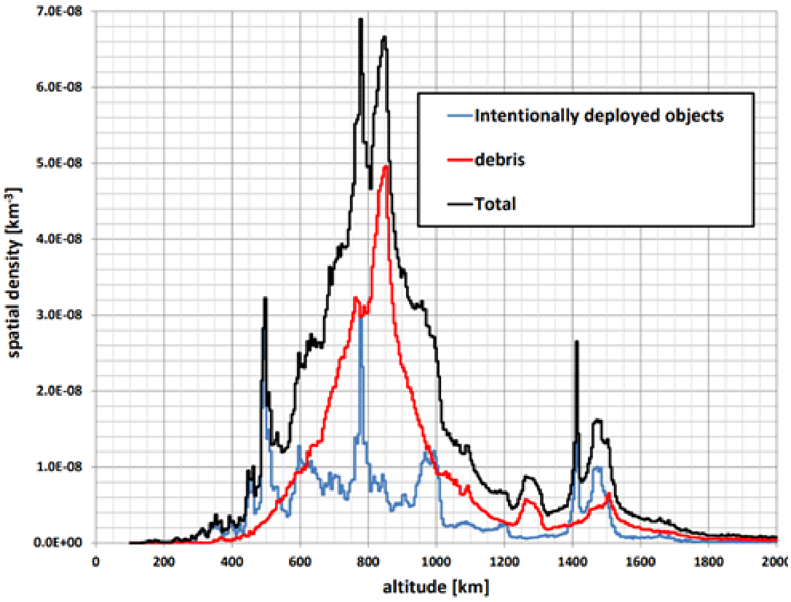

Figure 2.7: Altitude population up to 2000 km.

Two peaks can be seen at around 800 km, corresponding to the previously mentioned planned destruction of the Chinese satellite 'Fengyun-1C' in 2007 and the accidental collision between two satellites in 2009.

From this graph, it can be seen that in certain areas, there is a very high density, thus necessitating the implementation of space debris removal techniques.

2.1.2 Debris population at present

At the moment, as mentioned in previous chapters, the space surrounding the Earth is very crowded.

Below is a list containing the most essential data on the situation in orbit:[10]

- Number of rocket launches since the start of the space age in 1957 → **About 6020 (excluding failures).**
- Number of satellites these rocket launches have placed into Earth orbit → **About 10680.**
- Number of these still in space → **About 6250.**
- Number of these still functioning → **About 3600.**

- Number of debris objects regularly tracked by Space Surveillance Networks and maintained in their catalogue → **About 28210.**
- Estimated number of break-ups, explosions, collisions, or anomalous events resulting in fragmentation → **More than 550.**
- Total mass of all space objects in Earth orbit → **More than 9200 tonnes.**
- Number of debris objects estimated by statistical models to be in orbit:
  - **34000 objects greater than 10 cm.**
  - **900000 objects from ranging from 1 cm to 10 cm.**
  - **128 million objects ranging from 1 mm to 1 cm.**

2.1.3 Debris Catalogation

So far, the quantity of debris in space has been discussed and it can be imagined since the birth of debris there has been a need to detect, identify, catalogue and classify it. Radar, optical telescopes and infrared technology are used to monitor and characterise debris as required. Radar is generally used for debris in LEO orbits, optical sensors for GEO orbits and infrared observation techniques are usually used when the object's temperature needs to be known. The US has developed various systems to monitor space. The main objective was to keep an eye on other countries and identify possible missile attacks. As debris and space activity increased, the purpose became to monitor all launches and distinguish decaying satellites from possible hostile attacks.

Space Surveillance Network (SSN)

On 30 November 1957, the Space Surveillance Network was born with the project 'Harvest Moon'. As described in [11], the United States Space Surveillance Network involves detecting, tracking, cataloguing, and identifying artificial objects orbiting the Earth; e.g., active and inactive spacecraft, spent rocket bodies, mission-related debris, and fragments.

Space surveillance accomplishes the following:

- Predict when and where a decaying space object will reenter the Earth's atmosphere.
- Determines which country is responsible for an orbiting or reentering space object.
- Produce a running catalog of artificial space objects.

- Chart the present position of space objects and plot their anticipated trajectories.
- Detect new man-made objects in space.
- Inform NASA whether or not objects may interfere with the International Space Station or satellite orbits.

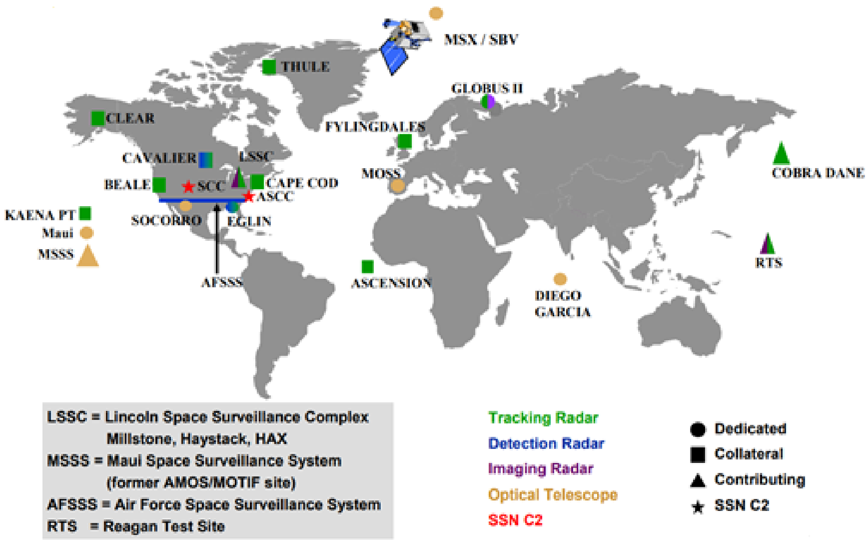

Figure 2.8: Space Surveillance Network map.

US Space Catalog

After the launch of 'Sputnik-1' in 1957, the United States Department of Defense (DoD) started to catalogue every satellite state in a database called *Space Catalog*. The SSN regularly updates the state of the satellites. To date, as mentioned in section 2.1.2, the number of catalogued objects is almost 28000.[12] The General Perturbations (GP) theory is used to maintain this catalogue, which provides a general analytical solution for the satellite equations of motion. The assumptions and approximations that are made in this model will be explained and deepened in section 3.2.

Space Situational Awareness program (SSA)

Space Situational Awareness Program (SSA) is a surveillance system of the European Space Agency. It aims to make Europe independent in detecting, tracking and monitoring artificial and non-artificial objects that could damage orbiting satellites and ground infrastructures.

It is divided into three main areas as described in [13]:

- Space Weather Segment (SWE) → monitoring and predicting the state of the Sun and the interplanetary and planetary environments, including Earth's magnetosphere, ionosphere and thermosphere, which can affect spaceborne and ground-based infrastructure thereby endangering human health and safety.
- Near-Earth Objects (NEO) → detecting natural objects such as asteroids that can potentially impact Earth and cause damage.
- Space Surveillance and Tracking (SST) → watching for active and inactive satellites, discarded launch stages and fragmentation debris orbiting Earth.

The SST completely covers the Earth's orbits (LEO, MEO, GEO) and compiles a catalogue containing all data related to the monitored objects.

2.1.4 Debris Classification

As previously mentioned, in orbit, there are many objects that are too small to be detected, in addition to the objects that our surveillance systems can detect. To classify the objects that are catalogued, they are divided into three categories:

- *Large Debris* → This category includes all debris with a size greater than about 10 cm in diameter. They represent the most catalogued category and are mostly concentrated in LEO orbit (less than 2000 km altitude), at about 20000 km and in GEO orbit (36000 km). Few objects are catalogued in orbit above 40000 km. It should be noted that below 2000 km, the majority of large debris is due to fragmentation. Between 2000 km and 16000 km payload debris is predominant, while above 16000 km, the majority is rocket debris.
- *Medium Debris* → This category includes all medium-sized objects ranging from about 1 mm to 10 cm in diameter. Debris of this size is only catalogued if it is in low orbit by ground-based surveys due to instrument limitations. Since medium-sized debris can be expected to come from large debris, it is approximated that these are on the same orbits. However, medium-sized debris is more affected by atmospheric drag and therefore undergoes a more rapid orbital decay. Although the amount and precise location of this category of debris is an estimate, it is known that it is derived from mission-related debris, payload debris and fragmentation debris.

- *Small Debris* → This category is represented by debris less than 1 mm in diameter and accounts for the majority of debris in orbit. All data are approximate estimates. As medium-sized debris is derived from mission-related debris, fragmentation debris (due to breakage) or deterioration of the satellite surface. Analyses show that almost 100% of this debris reenter the atmosphere after one year because it has a higher cross-sectional area ratio to mass and is more affected by atmospheric drag and solar pressure.

It should be noted that all data concerning high altitudes are not necessarily true as the sensors may not be able to detect all objects.

2.2 Overview of debris removal methods

It was calculated in the 2000s that by not performing any further launches for 100 years, the number of objects in orbit would still increase (as Kessler said) due to increasingly frequent collisions. As mentioned in the previous sections, measures to reduce the population of debris in Earth orbit are becoming increasingly crucial for the future of upcoming space missions. To date, various methods to mitigate the space debris problem are being investigated. Mitigation strategies aim to solve the debris problem in the long term. These are measures that minimise the production of debris that would add to the current population already in orbit or reduce the current population by actively influencing the structure of the debris. In the first case, known as passive mitigation, manufacturing techniques and proper planning of mission strategies are involved; in the second case, known as active mitigation, an external system is used to apply a force to the debris to manoeuvre it and possibly destroy it completely.

As better described in [11], the following techniques are the most important.

The two passive techniques are:

- *Passivation* → Consists of rendering spacecraft, rockets and their components devoid of any energy source onboard. Typical passivation measures include venting or burning excess propellant, discharging batteries and relieving pressure vessels.

- *Prevention* → This category includes: *Collision Avoidance* manoeuvres performed if the satellite is at a dangerous distance from another object, optimal mission planning and protection systems using protective shields.

The two active techniques are:

- *Re-orbiting* → This method consists of moving spacecraft into storage orbits with the same techniques used for de-orbiting (described below).

- *De-orbiting* $\rightarrow$ It is the most effective category and includes several strategies that can be used:
  - Natural decay: it is a passive method and depends on the aerodynamic resistance acting on the satellite. This method is used on satellites in low orbits (below 500 km).
  - End-of-life systems: this consists of projecting the satellite for an atmospheric re-entry manoeuvre at the end of its operational life. It can occur via chemical propulsion (less time but less efficient), and via electric propulsion (slow but more efficient).
  - Drag Augmentation systems: this category includes drag balloons and drag sails, which exploit viscous friction for satellite de-orbiting.
  - Robotic capture or through de-orbiting kit: is the most widely accepted solution currently being analysed in this thesis. A vehicle chaser reaches the target debris by performing a rendezvous manoeuvre and applies a de-orbiting kit which can be chosen from drag augmentation devices or end-of-life systems. If the robotic capture strategy is used, the debris can also be delivered to other vehicles already in orbit. To make this method of active debris removal (ADR) more efficient, the kit can be delivered to more debris as studied in this elaborate.
  - Other strategies: removal methods using foam, harpoons, nets, which are thrown from a certain distance, without the need to perform the rendezvous manoeuvre.

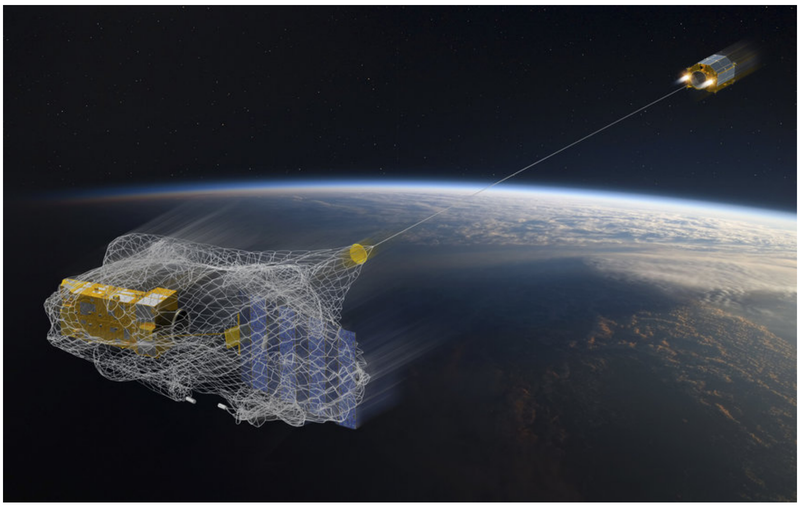

Figure 2.9: ADR through capture net.

Chapter 3

Mathematic model

3.1 Orbital Mechanics

Space debris in object can be described as satellites orbiting around the earth and they follow the same laws. We can approximate their motion with Newton two-bodies problem where a body with mass M exercises a gravitational force on a second body with a smaller mass m. The biggest body could be the Sun (or Earth), and the smaller one could be the Earth (or a satellite). So the hypothesis are:

- Smaller mass m « bigger mass M.
- Point-like bodies.
- Only gravitational forces.

Celestial Mechanics, astrodynamics and the design of any space mission are based on ***Kepler's laws of planetary motion***:

- The orbit of a planet is an ellipse with the Sun at one of the two foci.
- A line segment joining a planet and the Sun sweeps out equal areas during equal intervals of time.
- The square of a planet's orbital period is proportional to the cube of the length of the semi-major axis of its orbit.

$$F_M = F_m = G\frac{Mm}{r^2} \tag{3.1}$$

Where $G = 6.67 \times 10^{-11} \frac{Nm^2}{\mathrm{kg}^2}$ is the *Universal gravitational constant* and F_M, F_m are attraction forces. Knowing from Newton's second law: $\vec{F} = m\ddot{\vec{r}}$.

$$\begin{cases} m\ddot{\vec{\rho}} = -G\frac{Mm}{r^2} \times \frac{\vec{r}}{r} \\ M\ddot{\vec{R}} = G\frac{Mm}{r^2} \times \frac{\vec{r}}{r} \end{cases} \tag{3.2}$$

$\vec{r}$ is the vector connecting M and m.
By semplifing and subtracting equations it can be obtained the *relative acceleration* $\ddot{\vec{r}}$:

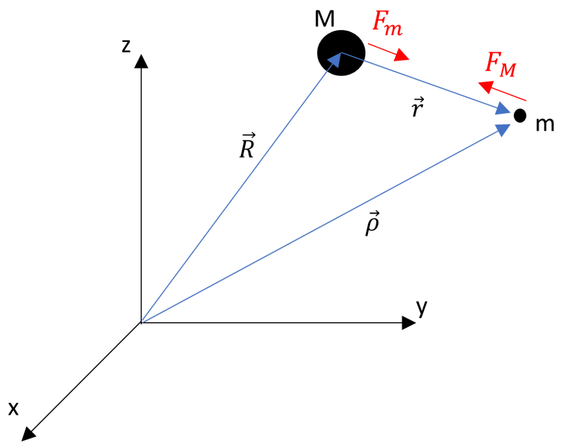

Figure 3.1: Two-body problem.

$$\ddot{\vec{r}} = \ddot{\vec{\rho}} - \ddot{\vec{R}} = -G\frac{(M+m)}{r^2} \times \frac{\vec{r}}{r} \tag{3.3}$$

where m is negligible.

It can be defined $\mu = GM$ and finally obtain the motion equation of the smaller body respect to the bigger:

$$\ddot{\vec{r}} + \frac{\mu}{r^2} \times \frac{\vec{r}}{r} = 0 \tag{3.4}$$

3.1.1 Angular Momentum

An important variable is *angular momentum* $\vec{h}$ because it relates the position and velocity of the secondary body respect to the principal body.

$$a_t = 2\dot{r}\dot{\nu} + r\ddot{\nu} = 0 = \frac{1}{r}\frac{d}{dt}(r^2\dot{\nu}) \tag{3.5}$$

ν is the angle between periapsis and the vector $\vec{r}$.
If derived equals to 0 so $(r^2\dot{\nu}) = cost$

$$(r^2\dot{\nu}) = r \times r\dot{\nu} = cost \tag{3.6}$$

Knowing that $r\dot{\nu} = v_t$:

$$rv_t = cost \tag{3.7}$$

And looking at figure 3.2:

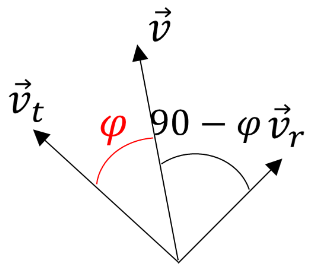

Figure 3.2: Speed components.

$$v_t = v\cos\varphi \tag{3.8}$$

Where φ is *flight path angle*.

$$rv\cos\varphi = cost \tag{3.9}$$

Multiplying equation 3.4 by r, a product between two parallel vectors is found:

$$\vec{r} \wedge \ddot{\vec{r}} = -\frac{\mu}{r^3}(\vec{r} \wedge \vec{r}) \tag{3.10}$$

The first term equals to:

$$\vec{r} \wedge \ddot{\vec{r}} = \frac{d}{dt}(\vec{r} \wedge \dot{\vec{r}}) = \dot{\vec{r}} \wedge \dot{\vec{r}} + \vec{r} \wedge \ddot{\vec{r}} = 0 \tag{3.11}$$

So:

$$\vec{r} \wedge \dot{\vec{r}} = cost \tag{3.12}$$

Can be defined the *angular momentum* $\vec{h} = \vec{r} \wedge \dot{\vec{r}} = \vec{r} \wedge \vec{v} = cost$:

$$|\vec{h}| = rv\sin(90-\varphi) = rv\cos\varphi \tag{3.13}$$

3.1.2 Mechanical Energy

The *Mechanical energy* can be obtained from equation 3.4:

$$\begin{matrix} a_t \Rightarrow \\ a_r \Rightarrow \end{matrix} \begin{cases} \ddot{r} - r\dot{\nu^2} = -\frac{\mu}{r^2} \\ 2\dot{r}\dot{\nu} + r\ddot{\nu} = 0 \end{cases} \tag{3.14}$$

a_r is *radial acceleration* and a_t is *tangential acceleration.* Multiplyng respectively by *radial velocity* $\dot{r}$ and by *tangential velocity* $r\dot{\nu}$ and summing them, the following result is obtained:

$$a_r\dot{r} + a_t r\dot{\nu} = -\frac{\mu}{r^2}r \tag{3.15}$$

$$\begin{gathered} \dot{r}\ddot{r} - r\dot{r}\dot{\nu^2} + 2r\dot{r}\dot{\nu^2} + r^2\dot{\nu}\ddot{\nu} = \frac{\mu}{r^2}\dot{r} \\ \dot{r}\ddot{r} - r\dot{r}\dot{\nu^2} + r^2\dot{\nu}\ddot{\nu} = \frac{\mu}{r^2}\dot{r} \end{gathered} \tag{3.16}$$

Now deriving equation 3.16:

$$\frac{1}{2}\frac{d}{dt}(\dot{r^2}) + \frac{1}{2}\frac{d}{dt}(r^2\dot{\nu^2}) = \frac{d}{dt}\frac{\mu}{r} \tag{3.17}$$

$$\frac{1}{2}\frac{d}{dt}(v_r^2 + v_t^2) = \frac{1}{2}\frac{d}{dt}\frac{\mu}{r} \tag{3.18}$$

Mechanical Energy E_g equation is obtained:

$$E_g = \frac{v^2}{2} - \frac{\mu}{r} = cost \tag{3.19}$$

Note that for ellipse and circle the *Mechanical Energy* is always $E_g < 0$.

3.1.3 Ellipse

An *ellipse* is obtained as the interseption of a cone with an inclined plane. It is a plane curve surrounding two focal points, such that for all points of the curve, and the sum of the two distances to the focal points is a constant.

The equation of the ellipse centered in the origin is represented in Cartesian form:

$$\frac{x^2}{a^2} + \frac{y^2}{b^2} = 1 \tag{3.20}$$

From this equation some important parameters can be described:

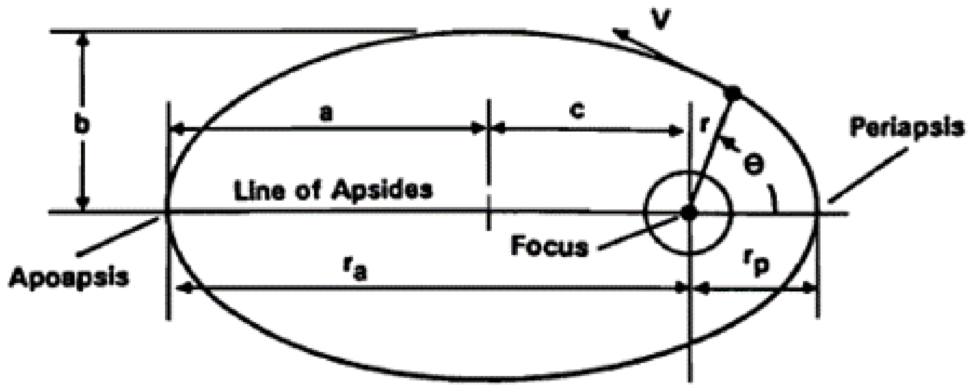

Figure 3.3: Elliptical orbit

- $a \rightarrow$ *semi-major axis*
- $b \rightarrow$ *semi-minor axis*
- $c = \sqrt{a^2 - b^2} \rightarrow$ *focal half distance.* The distance between one focus and center.
- $e \rightarrow$ *eccentricity.* The elongation of an ellipse is measured by its eccentricity e, a number ranging from $e = 0$ (the limiting case of a circle) to $e = 1$ (the limiting case of infinite elongation, no longer an ellipse but a parabola).

From these parameters, other important parameters of an elliptical orbit can be obtained: *perigee* and *apogee*, respectively, the nearest point of the orbit from the Earth (Earth is one of the focal points) and the farthest point.

Radius of Perigee:

$$r_{pe} = a - c = a - ae = a(1 - e) \tag{3.21}$$

Radius of Apogee:

$$r_{ap} = a + c = a + ae = a(1 + e) \tag{3.22}$$

As described in [14], an orbit is defined by its *orbital parameters*:

- $\nu \rightarrow$ *true anomaly*: defines the position of a body moving along a Keplerian orbit. It is the angle between the direction of periapsis and the body's current position, as seen from the main focus of the ellipse (the point around which the object orbits).

- $\psi \rightarrow$ *eccentric anomaly*: is given by the angle between the line of apses and the line between the geometric center of the ellipse and the projection of the planet on the auxiliary circle of radius equal to the semi-major axis of the ellipse.

$$\cos\psi = \frac{e + \cos\nu}{1 + e\cos\nu} \tag{3.23}$$

- $M \rightarrow$ *mean anomaly*: is the angular distance from the pericenter which a fictitious body would have if it moved in a circular orbit, with constant speed, in the same orbital period as the actual body in its elliptical orbit. *Mean anomaly* does not measure an angle between any physical objects. It is simply a convenient uniform measure of how far around its orbit a body has progressed since pericenter. [15][16] To define *mean anomaly* we need to introduce *mean motion* n because a body orbits along an orbit with a non-constant velocity.

$$n = \sqrt{\frac{\mu}{a^3}} \tag{3.24}$$

  From *mean motion* it can be obtained the *orbital period* T:

$$T = \frac{2\pi}{n} = 2\pi\sqrt{\frac{a^3}{\mu}} \tag{3.25}$$

  Which is proved in *Kepler's third law of planetary motion*, as in section 3.1.6.

A is defined as:

$$A = \frac{abM}{2} \tag{3.26}$$

Whenever A is equal to 2π the area swept by the vector ray coincides with the area of the ellipse πab. The time derivative of mean anomaly is constant for the *Kepler's second law of planetary motion*, and it is equal to mean motion:

$$\dot{A} = n = \sqrt{\frac{\mu}{a^3}} \tag{3.27}$$

We can also define mean anomaly as:

$$M = n\Delta t_{pe} = \psi - e\sin\psi \tag{3.28}$$

Where $\Delta t_{pe} \rightarrow$*time elapsed from the passage to the perigee* and it is equal to:

$$\Delta t_{pe} = \sqrt{\frac{a^3}{\mu}}\left[2\arctan\left(\sqrt{\frac{1-e}{1+e}}\tan\left(\frac{\nu}{2}\right)\right) - \frac{e\sqrt{1-e^2}\sin\nu}{1+e\cos\nu}\right] \tag{3.29}$$

Other parameters of the orbit are:

- p →*semilatus rectum*: the half length of the chord through one focus, perpendicular to the major axis.

$$p = a(1 - e^2) = \frac{h^2}{\mu} \tag{3.30}$$

- r →*vector ray*: on a generic point is the vector joining center of principal and center of secondary body, or connecting one focus of the orbit with one point along the orbit.

$$r = \frac{p}{1 + e\cos\nu} = \frac{a(1 - e^2)}{1 + e\cos\nu} = a(1 - e\cos\psi) \tag{3.31}$$

- V →*orbital speed*: on a generic point, is the speed of the body respectively to the center of mass.

$$V = \sqrt{\frac{\mu(1 + e^2 + 2e\cos\nu)}{a(1 - e^2)}} = \sqrt{\frac{\mu}{a}\frac{1 + e\cos\psi}{1 - e\cos\psi}} \tag{3.32}$$

For a specific point on the orbit we can describe *orbital speed* at *perigee* and *apogee*:

$$V_{pe} = \sqrt{\frac{\mu}{a}\frac{1 + e}{1 - e}} \tag{3.33}$$

$$V_{ap} = \sqrt{\frac{\mu}{a}\frac{1 - e}{1 + e}} \tag{3.34}$$

We define now three angles that are very important for the definition of an orbit (see figure 3.4):

- Ω →*longitude of the ascending node*: it is the angle from a specified reference direction, called the origin of longitude, to the direction of the ascending node, as measured in a specified reference plane. The ascending node is the point where the orbit of the object passes through the plane of reference. see image and cit.

- i →*orbital inclination*: it is expressed as the angle between a reference plane and the orbital plane or axis of direction of the orbiting object. see image and cit.

- ω →*argument of periapsis*: it defines the orientation of the ellipse in the orbital plane as an angle measured from the ascending node to the periapsis. see image and cit.

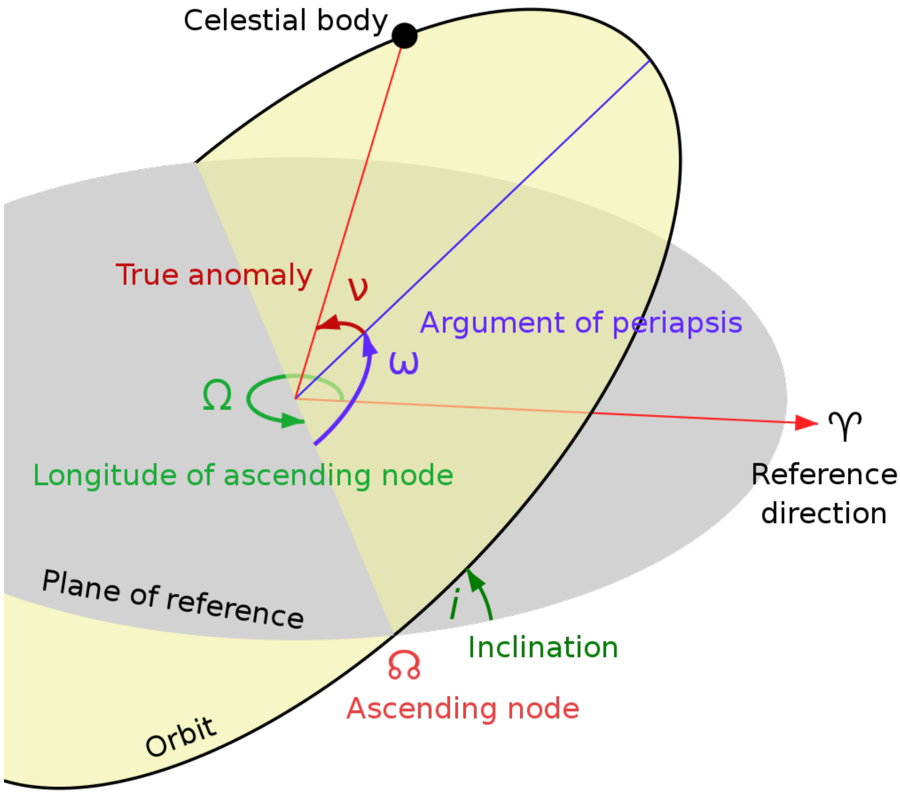

Figure 3.4: Orbital angles.

3.1.4 Orbital elements

Orbital elements are the six parameters that we need to identify a specific unique orbit:

- e →*eccentricity*
- a →*semi-major axis*
- Ω →*longitude of the ascending node*
- ω →*argument of periapsis*
- ν →*true anomaly*
- i →*inclination*

3.1.5 Kepler's second law of planetary motion

Looking for a relation between *true anomaly* ν and *time* it can be obtaied *Kepler's second law of planetary motion*:

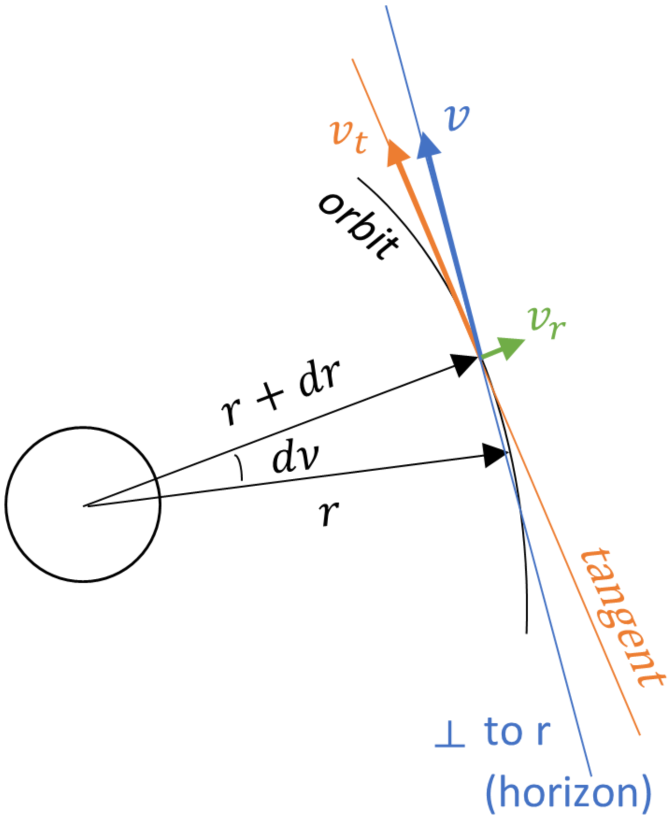

Figure 3.5: Motion of a body - Speed components.

Knowing that:

$$V_t = r\dot{\nu} \tag{3.35}$$

$$h = rv_t = r^2\dot{\nu} \tag{3.36}$$

$$\dot{\nu} = \frac{d\nu}{dt} = \frac{h^2}{2} \tag{3.37}$$

For a circular sector:

$$A_\nu = \pi r^2 \frac{\nu}{2\pi} = \frac{r^2 \nu}{2} \tag{3.38}$$

$$dA = \frac{r^2}{2} d\nu \tag{3.39}$$

Dividing by dt:

$$\frac{1}{dt} A = \frac{r^2}{2} d\nu \frac{1}{dt} \Rightarrow \frac{dA}{dt} = \frac{r^2}{2} \dot{\nu} \tag{3.40}$$

Is obtained *Kepler's second law of planetary motion*:

$$dt = \frac{2}{h} dA \tag{3.41}$$

This formula demonstrates Kepler's second law of planetary motion.

3.1.6 Kepler's third law of planetary motion

Starting from the *second law* to demonstrate *Kepler's third law of planetary motion* :

$$\frac{dA}{dt} = \frac{h}{2} = cost = \frac{A_E}{\tau_E} \tag{3.42}$$

$$\tau_E = A_E \frac{2}{h} \tag{3.43}$$

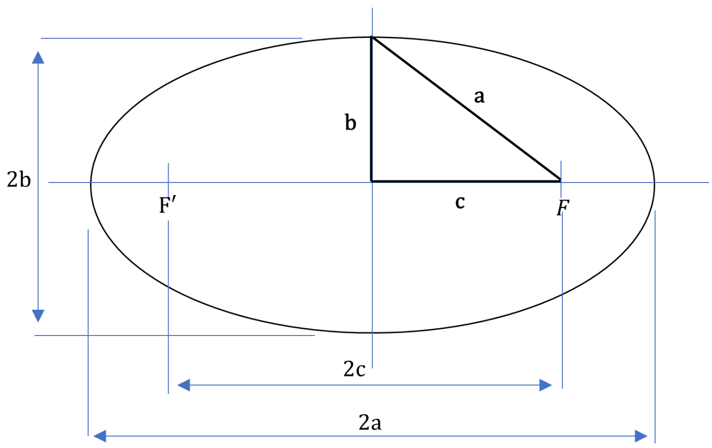

Figure 3.6: Ellipse.

Knowing from an ellipse as in figure 3.6:

$$A_E = \pi ab \tag{3.44}$$

$$b = \sqrt{a^2 - c^2} \tag{3.45}$$

$$c = ae \tag{3.46}$$

$$\Rightarrow b = \sqrt{a^2(1 - e^2)} = a\sqrt{1 - e^2} \tag{3.47}$$

The *angular momentum* can be derived from equation 3.30:

$$h = \sqrt{\mu a(1 - e^2)} \tag{3.48}$$

Putting together in equation 3.43 it is obtained *Kepler's third law of planetary motion*:

$$\tau_E = 2\frac{\pi a a\sqrt{1 - e^2}}{\sqrt{\mu a(1 - e^2)}} = 2\pi\sqrt{\frac{a^3}{\mu}} \tag{3.49}$$

3.2 Orbital perturbations

Keplerian orbits are ideal. In reality, the motion of bodies (artificial or natural) orbiting around a planet is perturbed by some phenomena that modify their trajectories. So this *orbital perturbations* can modify *orbital parameters* more or less significantly depending on trajectory and body characteristics. Therefore in a determinate moment, a body should be on a Keplerian orbit, but it is on a real orbit as we can see in figure 3.7.

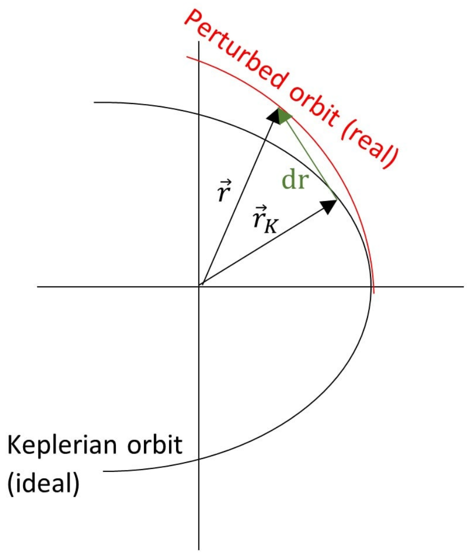

Figure 3.7: Keplerian and Perturbed orbit - Encke's method.

There are two ways to solve the problem of orbital perturbations:

- *General perturbation method*: solved analytically, using variation of orbital element or variation of constant of integration.
- *Special perturbation method*: numerical solution, can be applied to any problem in celestial mechanics.

$$d\vec{r} = \vec{r} - \vec{r_K} \tag{3.50}$$

$$d\dot{\vec{r}} = \dot{\vec{r}} - \dot{\vec{r_K}} \tag{3.51}$$

$$d\ddot{\vec{r}} = \ddot{\vec{r}} - \ddot{\vec{r_K}} \tag{3.52}$$

$$\Rightarrow d\ddot{\vec{r}} = -\mu\left(\frac{\vec{r}}{r^3} - \frac{\vec{r_K}}{r_K^3}\right) + \vec{a_p} \tag{3.53}$$

This perturbation phenomena are classified in different categories in relation to how much they depend on time. All parameters have a drifting in time so:

- *Secolar perturbations*: in first approximation are proportional to time and they cause a continuous increase or decrease of the parameter on which they act. If considering a finite time interval, they can be considered linear in time. They are for example *solar pressure* and *aerodinamic drag*, with non-conservative fields.

- *Resonant perturbations*: they cause harmonic variations of orbital parameters.

- *Long period periodical perturbations*: they cause harmonic variations.

  – Geopotential perturbations: similar in quantity to rotation period of perihelion.

  – Presence of Sun and Moon: order of months or years.

- *Short period periodical perturbations*: they cause harmonic variations of orbital parameters similar in quantity to orbital period of the body.

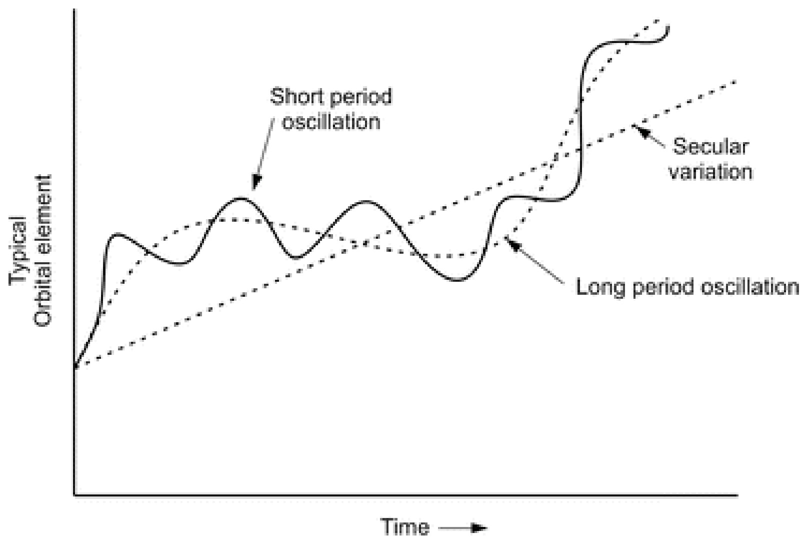

Figure 3.8: Secolar and periodic perturbations.

Perturbations that depends on gravitational potential have a periodic and conservative nature like third-body perturbation or oblateness of the Earth. Classical theory shows that orbital elements a, e and i are subject exclusively to periodic perturbations. Instead, Ω, ω and M are subject to both periodic perturbations and secular perturbations.

Pherturbing phenomena are:

$$\textbf{Gravitational} \Rightarrow \begin{cases} \textit{Third-body perturbation} \\ \textit{Earth's gravitational asymmetries} \end{cases}$$

$$\textbf{Non-gravitational} \Rightarrow \begin{cases} \textit{Atmosferic drag} \\ \textit{Solar pressure} \end{cases}$$

3.2.1 Earth's gravitational asymmetries

Two-body Keplerian model provides that the attractor body (Earth) is perfectly spherical, with a homogeneous distribution of density. But planet Earth in reality is not spherical and does not have a homogeneous distribution of mass:

- *Oblateness*$= \frac{1}{298.2} \rightarrow$ is defined as difference between equatorial and polar radius divided by equatorial radius.
- *Eccentricity at equator*$= 1.14 \times 10^{-5} \rightarrow$ is defined as ratio between half-focal distance and semi-major axis.

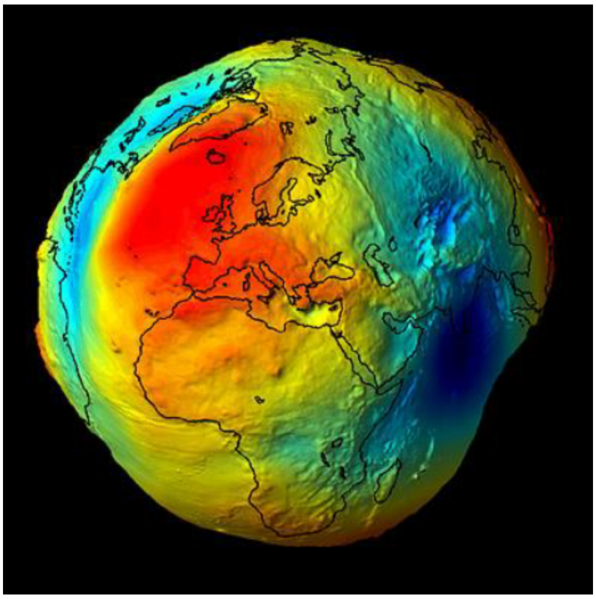

Figure 3.9: Geoid: perpendicular surface at gravity in every point.

- Difference between equatorial and polar radius is about 21384 *km*.
- Difference between semi-major axis and semi-minor axis at equator is about 145 *m*.

This clear diversity, as seen in figure 3.9, between the Keplerian model and the real characteristics of planet Earth is the main reason of perturbative action caused by Earth's gravitational asymmetries. To define a more realistic Earth's gravity field, we define a semi-analytic model of gravitational energy, taking account of Earth's oblateness, ellipticity at equator and other differences between Earth's real gravity field and spherical gravitational field. The expression for gravitational energy (potential) that does not have any spherical symmetry is:

$$U(r,\lambda,\delta) = \frac{\mu_E}{r}\left[1-\sum_{n=2}^{\infty}\sum_{m=0}^{n}\left(\frac{R_E}{r}\right)^n[C_{nm}\cos(m\lambda)+S_{nm}\sin(m\lambda)]P_{nm}(\sin\delta)\right] \quad (3.54)$$

With:

- μ_E: *standard gravitational parameter.*
- r: *radial distance deetween center of mass of the two bodies.*
- R_E: *Earth's equatorial radius.*
- n: *harmonic degree.*
- m: *harmonic order.*
- λ: *longitude.*
- δ: *declination.*
- C_{nm}, S_{nm}: *coefficients.*
- P_{nm}: *associated Legendre polynomials.*

$$P_{mn}(x) = \frac{1}{2^n n!}\frac{d(1-x^2)^{\frac{m}{2}}}{dx}\frac{d^{n+m}(x^2-1)^n}{dx^{(n+m)}} \quad (3.55)$$

Expressions of associated Legendre polynomials P_{nm} and coefficients C_{nm}, S_{nm} are normalized as follows:

$$\bar{C}_{nm} = \sqrt{\frac{(n+m)!}{(2n+1)k(n-1)!}}C_{nm} \quad (3.56)$$

$$\bar{S}_{nm} = \sqrt{\frac{(n+m)!}{(2n+1)k(n-1)!}} S_{nm} \tag{3.57}$$

$$\bar{P}_{nm} = \sqrt{\frac{(2n+1)k(n-1)!}{(n+m)!}} P_{nm} \tag{3.58}$$

With:

$$k = \begin{cases} 1 & \text{if} \quad m = 0 \\ 2 & \text{if} \quad m \neq 0 \end{cases}$$

Normalized coefficients $\bar{C}_{nm}$, $\bar{S}_{nm}$ can be found in appropriate lists function of degree n and order m. Comparing equation 3.2.1 with gravitational energy associated to ideal model (Earth perfectly spherical):

$$U = \frac{\mu_E}{r} \tag{3.59}$$

It can be found *perturbative potential* that defines differences netween the two models:

$$V(r, \lambda, \delta) = \frac{\mu_E}{r} \sum_{n=2}^{\infty} \sum_{m=0}^{n} \left(\frac{R_E}{r}\right)^n [C_{nm} \cos{(m\lambda)} + S_{nm} \sin{(m\lambda)}] P_{nm}(\sin\delta) \tag{3.60}$$

The gravitational field described by equation 3.60 is divided into positive and negative potential zones, depending on the values assumed by n and m. P_{nm} is equal to zero on the boundary lines between these zones. According to the values assumed by n and m, the following nomenclature is used for experimental coefficients C_{nm} and S_{nm}:

- *Zonal spherical harmonics* : $m = 0 \rightarrow$ potential is no longer dependent on longitude. As we can see in figure 3.10, in this case exists n latitude circles where P_{nm} is equal to zero. Consequently the field is divided in $n + 1$ zones, with alternating signs (+ and −).

- *Sectoral spherical harmonics* : $m = n \rightarrow P_{nm}$ values are equal to zero for 2n values of the longitude, the field is therefore divided by 2n lines with constant longitude, which define 2n “segments” with alternating values of the P_{nm} function.

- *Tesseral spherical harmonics* : $m \neq n \rightarrow$ alternating zones for the P_{nm} function are arranged in a "tile" configuration square.

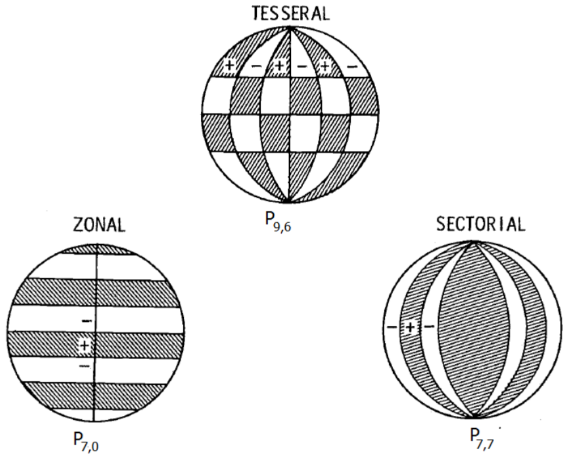

Figure 3.10: P_{nm} as m, n vary - Harmonics.

For zonal spherical harmonics is defined:

$$C_{n,0} = C_n = -J_n \tag{3.61}$$

The table below shows the values of the zonal harmonics J_n up to $n = 7$; notice how the harmonic J_2 is about 400 times larger than the next harmonic, J_3.

Harmonic	**Value**
j_2	$+1.0826 \times 10^{-3}$
j_3	-2.5327×10^{-6}
j_4	-1.6196×10^{-6}
j_5	-2.2730×10^{-7}
j_6	$+5.4868 \times 10^{-7}$
j_7	-3.5236×10^{-7}

Table 3.1: Values of zonal harmonics up to J_7.

Calculating the gradient of equation 3.60, the expression of the components of the perturbative acceleration due to the Earth's gravitational field asymmetries is obtained:

$$a_p = \nabla V \tag{3.62}$$

Obtaining components:

$$a_r = \frac{\mu}{r^2}V - \frac{\mu}{r}\sum_{n=2}^{\infty}\sum_{m=0}^{n}\Big(-n(R_E)^n r^{-(n+1)}\Big)\Big(C_{nm}\cos(m\lambda) + S_{nm}\sin(m\lambda)\Big)C_{nm}\sin(\delta) \tag{3.63}$$

$$a_\lambda = \frac{\mu}{r^2}\frac{m}{\cos\delta}\left[\sum_{n=2}^{\infty}\sum_{m=0}^{n}\left(\frac{R_E}{r}\right)^n\Big(S_{nm}\cos(m\lambda) - C_{nm}\sin(m\lambda)\Big)P_{nm}\sin(\delta)\right] \tag{3.64}$$

$$a_\delta = \left[\left(\frac{1}{2^n n!}\frac{d(1-x^2)^{\frac{m}{2}}}{dx}\frac{d^{(n+m)}(1-x^2)^n}{dx^{n+m}} + \frac{(1-x^2)^{\frac{m}{2}}}{2^n n!}\frac{d^{n+m+1}(x^2-1)^n}{dx^{(n+m+1)}}\right)\cos\delta\right]\cdot$$
$$\frac{\mu}{r^2}\frac{\mu}{r}\left[\sum_{n=2}^{\infty}\sum_{m=0}^{n}\left(\frac{R_E}{r}\right)^n\Big(C_{nm}\cos(m\lambda) + S_{nm}\sin(m\lambda)\Big)\right] \tag{3.65}$$

From the values shown in table 3.2.1, as said before, J_2 is predominant compared to the other zonal harmonic. Harmonic J_2 is associated to Earth's oblateness, as shown in the figure 3.11.

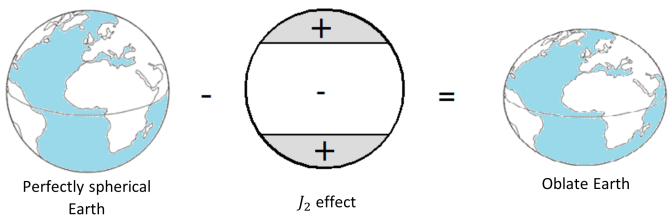

Figure 3.11: Effect of perturbative potential J_2.

After a few theorical steps it can be obtained the variations of *longitude of the ascending node*, *argument of perigee* and *mean anomaly*.

Effect of Earth's oblateness - nodal precession

$$\frac{d\Omega}{dt} = -\frac{3}{2}\left(\frac{r_E}{p}\right)^2 nJ_2\cos i \tag{3.66}$$

This phenomenon is called *nodal precession* and consists of a variation of the angle between the orbital plane and orbit inclination i. The expression 3.66 shows that:

- If $0 < i < \frac{\pi}{2} \Rightarrow$ *Regression*: angle between orbital plane and orbital inclination decreases.
- If $\frac{\pi}{2} < i < \pi \Rightarrow$ *Precession*: angle between orbital plane and orbital inclination increases.

Effect of Earth's oblateness - aspides precession

$$\frac{d\omega}{dt} = \frac{3}{4}\left(\frac{r_E}{p}\right)^2 nJ_2\left(5\cos^2 i - 1\right) \tag{3.67}$$

This phenomenon is called *apsidal precession* and consists of a gradual rotation of the line connecting the apsides (apogee and perigee). Looking at expression 3.67 it can be noticed that:

$$if \quad 5\cos^2 i - 1 = 0 \Rightarrow \cos i = \sqrt{\frac{1}{5}} \tag{3.68}$$

Then by solving the equation these solutions are obtained:

- $i = 63.4°$
- $i = 116.6°$

In these two cases, equation 3.67 is equal to zero, so it means that a satellite orbiting around Earth with $i = 63.4°$ or $i = 116.6°$ is not affected by this perturbation. We can even specify that:

- If $i < 63.4°$ or $i < 116.6°$ $\Rightarrow$ *Precession*: orbit's axis rotates in the same direction as the orbital motion.
- If $63.4° < i < 116.6°$ $\Rightarrow$ *Regression*: orbit's axis rotates in the opposite direction as the orbital motion.

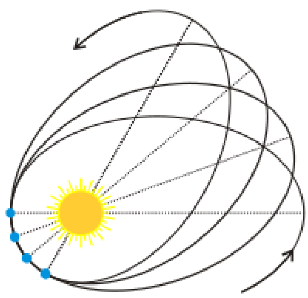

Figure 3.12: Apsidial precession.

Effect of Earth's oblateness on mean anomaly

$$\frac{dM}{dt} = n + \frac{3}{4}\left(\frac{r_E}{p}\right)^2 nJ_2\sqrt{1-e^2}\left(3\cos^2 i - 1\right) \tag{3.69}$$

3.2.2 Third-body perturbation

One of the hypotheses at the base of the formulation of the Keplerian two-body problem consists in considering the secondary body subjected to the gravitational action of the only primary body, neglecting the gravitational attraction of any other body of the space environment. This approximation becomes very heavy for satellites that operate in high orbits, but it cannot be neglected even for satellites that propagate for long periods in low orbits. For a realistic study of the motion of bodies around the Earth, it is necessary to consider the effect of the attraction of the Moon and the Sun.

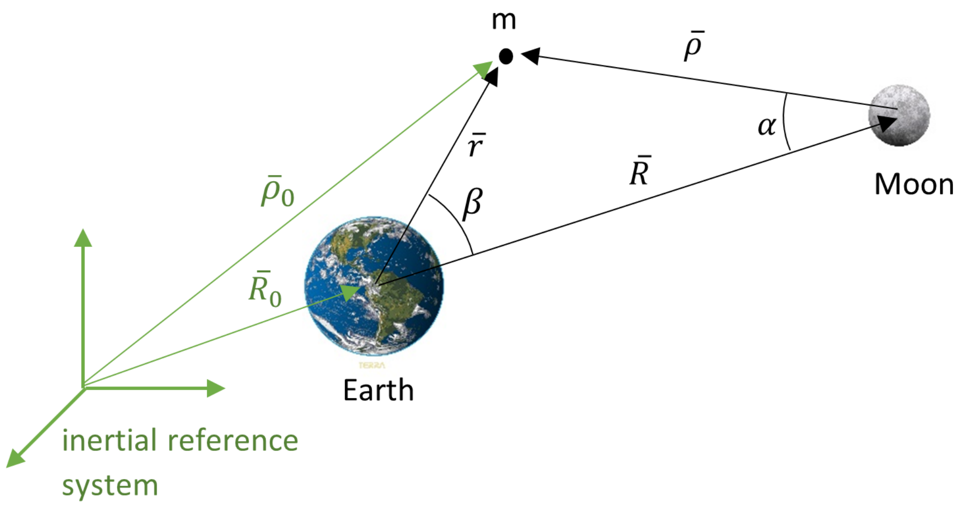

Figure 3.13: Earth, Moon and orbiting-body scheme.

It can be written:

$$\vec{R} = \vec{\rho}\cos\alpha + \vec{r}\cos\beta \tag{3.70}$$

$$\vec{r} = \vec{\rho}_0 - \vec{R}_0 \tag{3.71}$$

Systemizing the equations of the two bodies:

$$\begin{cases} m\ddot{\vec{\rho}}_0 = -G\frac{Mm}{r^2}\frac{\vec{r}}{r} - G\frac{mm_p}{\rho^2}\frac{\vec{\rho}}{\rho} \\ M\ddot{\vec{R}}_0 = +G\frac{Mm}{r^2}\frac{\vec{r}}{r} - G\frac{Mm_p}{R^2}\frac{\vec{R}}{R} \end{cases} \tag{3.72}$$

Where M is the mass of the Earth and m_p is the mass of the third-body (in this case the moon). Subtracting the second equation from the first:

$$\ddot{\vec{\rho}}_0 - \ddot{\vec{R}}_0 = -G\frac{(M+m)}{r^2}\frac{\vec{r}}{r} - G\frac{m_p}{\rho^2}\frac{\vec{\rho}}{\rho} + G\frac{m_p}{R^2}\frac{\vec{R}}{R} \tag{3.73}$$

Knowing that mass m is negligible, $\mu_E = GM, \mu_p = Gm$, it can be obtained the acceleration of the orbiting body relative to the Earth:

$$\ddot{\vec{r}} = -\frac{\mu_E}{r^2}\frac{\vec{r}}{r} - \frac{\mu_p}{\rho^2}\frac{\vec{\rho}}{\rho} + \frac{\mu_p}{R^2}\frac{\vec{R}}{R} \tag{3.74}$$

Where:

$$a_p = \frac{\mu_p}{R^2}\frac{\vec{R}}{R} - \frac{\mu_p}{\rho^2}\frac{\vec{\rho}}{\rho} = \mu_p\left[\frac{\vec{R}}{R^3} - \frac{\vec{\rho}}{\rho^3}\right] \tag{3.75}$$

a_p is the *perturbing acceleration.*

$$\Rightarrow \frac{a_p}{\mu_p} = \frac{\vec{R}}{R^3} - \frac{\vec{\rho}}{\rho^3} \tag{3.76}$$

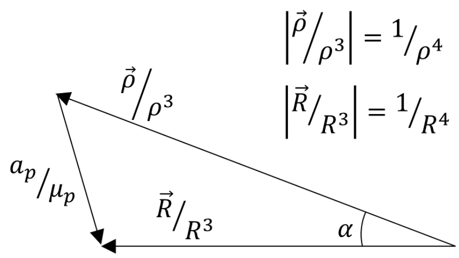

Applying Law of cosines:

$$a_p = \frac{\mu_p}{\rho^2}\sqrt{1 + \frac{\rho^4}{R^4} - \frac{2\rho^2}{R^2}\cos\alpha} \tag{3.77}$$

Looking at this expression it can be observed about distances ρ, R:

- If $\rho << R \Rightarrow a_p = \frac{\mu_p}{\rho^2}$ $\rightarrow$ It means that since the body is very close to the third body, the perturbative acceleration is given approximately only by the third body (the Moon in this case).

- If

$$\begin{cases} R_{Earth-Moon} = 384400km \\ r_{Geo-sat} = 42000km \end{cases}$$

$\rho \approx R$ so we can approximate $R >> r$. We obtain:

$$\frac{r}{R} << 1 \quad \Rightarrow \quad \frac{r}{R} = \varepsilon \tag{3.78}$$

From equation 3.70 we can write:

$$\cos\alpha = \frac{R - r\cos\beta}{\rho} \tag{3.79}$$

$$\frac{\rho}{R}\cos\alpha = -\frac{r}{R}\cos\beta + 1 = 1 - \varepsilon\cos\beta \tag{3.80}$$

Substituting in equation 3.77 the result found in equation 3.80, a_p can be evaluated with the following expression:

$$a_p = \frac{\mu_p}{\rho^2}\sqrt{1 + \frac{\rho^4}{R^4} - \frac{2\rho}{R}\Big(1 - \varepsilon\cos\beta\Big)} \tag{3.81}$$

Applying some mathematical simplifications and binomial theorem we obtain the formula of the perturbative acceleration when the perturbed body is close to the Earth:

$$a_p = \frac{\mu_p r}{R^3}\sqrt{1 + 3\cos\beta} \tag{3.82}$$

Two particular cases can be identified:

  - If $\beta = 0, \pi \quad \Rightarrow \quad a_p \cong 2\frac{\mu_p}{R^3}r \quad \rightarrow$ *Conjunction*: occurs when two astronomical objects or spacecraft have either the same right ascension or the same ecliptic longitude, usually as observed from Earth. In this case the pertubing action is maximum.[16][17]
  - If $\beta = \frac{\pi}{2}, \frac{3}{2}\pi \quad \Rightarrow \quad a_p \cong \frac{\mu_p}{R^3}r \quad \rightarrow$ *Quadrature*: is the configuration of a celestial object in which its elongation is perpendicular to the direction of the Sun. In this case the pertubing action is minimum.

Regarding the impact on orbital parameters, the gravitational attraction force exerted by the third body is however a conservative force (the third body is considered perfectly spherical), and consequently, we will not have dissipation of the mechanical energy, nor variations in the orbit form (it means that we will not have a variation of orbital parameters such as semi-major axis and eccentricity). The largest secular variations involve the longitude of ascending node and the argument of perigee, estimated as follows:

$$\frac{d\Omega_{Moon}}{dt} = -0.00338\frac{\cos i}{n} \tag{3.83}$$

$$\frac{d\Omega_{Sun}}{dt} = -0.00154\frac{\cos i}{n} \tag{3.84}$$

$$\frac{d\omega_{Moon}}{dt} = -0.00169\frac{4 - 5\sin^2 i}{n} \tag{3.85}$$

$$\frac{d\omega_{Sun}}{dt} = -0.00077\frac{4 - 5\sin^2 i}{n} \tag{3.86}$$

3.2.3 Atmosferic drag

Atmospheric drag is a particularly significant perturbation for low orbits. The precise calculation of the forces that are generated by the interaction of the orbiting body on contact with the surrounding atmosphere is affected by several uncertainties related to

- Shape and relative orientation of the satellite with respect to the surrounding atmosphere.
- Difficult to estimate the characteristics of the atmosphere at altitudes of interest for spaceflight, since they are variable due to solar and geomagnetic activity.
- Condition of rarefied air in the high atmosphere.
- Possible ionization of the atmosphere; can lead to a complex interaction between exposed surfaces and the surrounding atmosphere.

From the formulation of aerodinamic drag:

$$m\frac{dv}{dt} = -\frac{1}{2}\rho\omega^2 SC_D \tag{3.87}$$

Where: m is the mass of the body, $\omega^2 \cong v^2 = \frac{\mu}{a}$, v is speed, ρ is density, S is the section of the body perpendicular to the direction of motion, C_D is the aerodynamic drag coefficient.

In general, for satellites in orbit above 200 km altitude, the drag coefficient is about 2.2 for spherical bodies and about 3 for cylindrical bodies, assumes an intermediate value for the other possible shapes. As it is evident from the expression 3.87, the acceleration due to the atmospheric resistance depends explicitly on the density. Consequently, the choice of the atmospheric model to be used is crucial in order to obtain a good estimate of the effects of the atmosphere on the motion of the body. Regarding this, there are many models of the atmosphere, periodically updated, provided by agencies specialized in studying the space environment. Regarding the impact of the aerodynamic action on the orbital parameters, we must keep in mind that aerodynamic friction force is a dissipating force. Consequently, its action on the satellite causes a decrease of the body's mechanical energy. The mechanical energy is directly associated with the semi-major axis values through the relation:

$$E_g = -\frac{\mu}{2a} \tag{3.88}$$

Ultimately, the decrease in mechanical energy due to aerodynamic resistance results in a reduction of the semi-major axis and eccentricity of the orbit; as already discussed above, the semi-major axis and the eccentricity represent the orbital parameters that characterize the shape of the orbit. Consequently, we can say that the action of the atmospheric resistance modifies the orbit of the body. Specifically, both the semi-major axis and the eccentricity tend to decrease, determining a circularization of the orbit and a loss of altitude of the body. When the eccentricity is close to zero, the progressive decrease of the semi-major axis determines a spiral motion towards lower altitudes, which continues until the increasing atmospheric density leads to the fragmentation of the body, under the effect of thermal and mechanical loads.

A simple formulation of the perturbative acceleration due to aerodinamic drag, obtained from equation 3.87 and equation 3.88, is as follows:

$$a_{DRAG} = -\sqrt{\mu a}\frac{S}{m}\rho C_D \tag{3.89}$$

In this equation it can be identified an important parameter:

$$BC = \frac{m}{SC_D} \tag{3.90}$$

BC $\rightarrow$*Ballistic coefficient*: the measure of the ability of a body to overcome air resistance in flight.[18] The higher the ballistic coefficient, the less the body is affected by aerodynamic resistance.

3.2.4 Solar pressure

Solar pressure is a disturbance related to the force exerted on the outer surface of a satellite by electromagnetic radiation impinging on it. Physically, a wave (or electromagnetic radiation) is made up of magnetic and electric fields that oscillate perpendicular to each other and to the direction of propagation of the wave.

A simple formulation of the perturbative acceleration due to solar pressure is as follows:

$$a_{pres} = \frac{pS}{m} \tag{3.91}$$

S is the body's surface, m is the mass, and p is the solar pressure.

$$p_{1AU} = 4.5632 \cdot 10^{-6} \frac{N}{m^2} \tag{3.92}$$

This value of p is the *solar pressure* at 1 AU (*Astronomic unit* or Earth-Sun distance, about 150 Million km).

As already mentioned in the section 1, in this thesis, only perturbations derived from Earth's oblateness are taken into account.

3.3 Transfer maneuvers

A *transfer manoeuvre* consists of using a propulsion system to modify the speed vector, so to modify the orbit (or some of its parameters) of a spacecraft. There are various types of manoeuvres, and those useful for the calculations in this thesis will be discussed in more detail.

3.3.1 Hohmann transfer orbit

Hohmann transfer orbit is the most economical manoeuvre and requires a minimum change in speed ΔV. It allows a satellite to move from a circular orbit of radius r_1 to a coplanar orbit or radius r_2. The first impulsive speed variation ΔV_1 puts the satellite on an elliptical transfer orbit with pericenter r_1 and apocenter r_2. The second impulse ΔV_2 is performed after half a revolution and serves to circularize the final orbit.

A scheme of a *Hohmann transfer* is as follows:

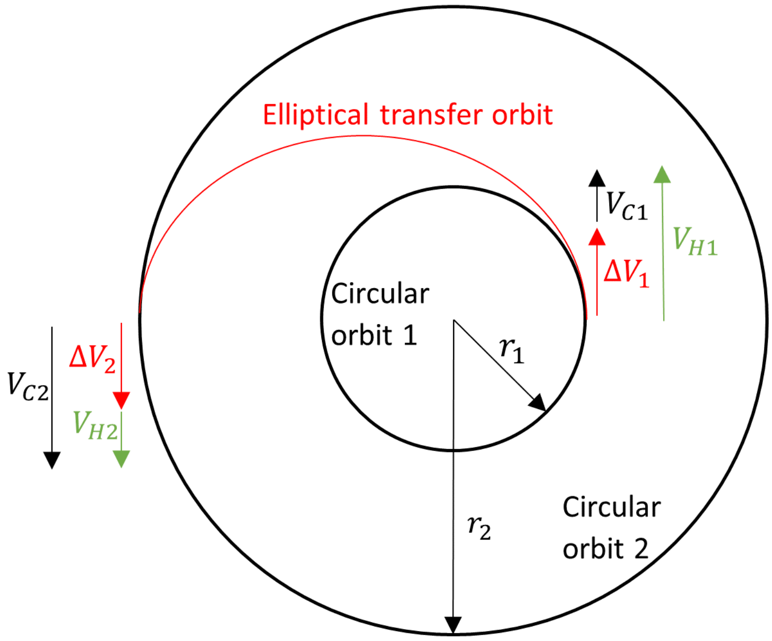

Figure 3.14: Hohmann transfer.

As mentioned above radius of perigee r_p and radius of apogee r_a are respectively radius of starting orbit r_1 and radius of arrival orbit r_2:

$$r_p = r_1 \tag{3.93}$$

$$r_a = r_2 \tag{3.94}$$

It can be obtained semi-major axis a_H and eccentricity e_H of the elliptical transfer orbit:

$$a_H = \frac{r_1 + r_2}{2} \tag{3.95}$$

$$e_H = \frac{r_2 - r_1}{r_1 + r_2} \tag{3.96}$$

As we can see in figure 3.14, the satellite orbiting on the circular orbit 1 has a circular speed V_{C1} to which ΔV_1 is added, obtaining maximum velocity V_{H1}. Satellite arrives on the apoapsis having minimum velocity V_{H2}, now second impulse ΔV_2 accelerates the satellite to circular speed V_{C2}.

$$V_{C1} = \sqrt{\frac{\mu}{r_1}} \tag{3.97}$$

$$V_{C2} = \sqrt{\frac{\mu}{r_2}} \tag{3.98}$$

Expressions of V_{H1} and V_{H2} of the transfer orbit can be obtained using equation of mechanical energy 3.19:

$$E_g = \frac{V^2}{2} - \frac{\mu}{r} = \frac{\mu}{2a} \tag{3.99}$$

Obtaining *Hohmann's Mechanical energy*:

$$E_H = -\frac{\mu}{2a_H} = -\frac{\mu}{r_1 + r_2} \tag{3.100}$$

So *Hohmann's velocities* are:

$$V_{H1} = \sqrt{2\Big(-\frac{\mu}{r_1 + r_2} + \frac{\mu}{r_1}\Big)} \tag{3.101}$$

$$V_{H2} = \sqrt{2\Big(-\frac{\mu}{r_1 + r_2} + \frac{\mu}{r_2}\Big)} \tag{3.102}$$

Therefore, ΔV cost of the first maneuver is:

$$\Delta V_1 = V_{H1} - V_{C1} = V_{C1}\left(\sqrt{\frac{2r_2}{r_1 + r_2}} - 1\right) > 0 \tag{3.103}$$

And ΔV cost of the second maneuver is:

$$\Delta V_2 = V_{C2} - V_{H2} = V_{C2}\left(1 - \sqrt{\frac{2r_1}{r_1 + r_2}}\right) > 0 \tag{3.104}$$

Obtaining the total cost of the maneuver:

$$\Delta V = |\Delta V_1| + |\Delta V_2| \tag{3.105}$$

In this example, the transfer is made from a circular orbit with a smaller radius to one with a larger radius through two increments (accelerations) of speed. However, if the transfer takes place from a larger circular orbit to a smaller one, two decreases (decelerations) are necessary. In this case, the pulses will be negative and not positive, as in the previous example. It must be pointed out that there are losses due to gravity, which have a more significant influence in the case of a small radius. Therefore, to spend a short time under the action of gravitational force, more giant pulses are recommended for small radius, while smaller pulses can be used for large radius. The transfer from one orbit to another becomes much more complicated if another orbiting object is to be intercepted. In fact, the interceptor, in this case the *chaser*, and the *target* (*debris*) must arrive at the *rendezvous point* at the same moment. This common manoeuvre is called *space rendezvous*, and it consists of a set of orbital manoeuvres that leads to an encounter of two bodies orbiting.

As mentioned, *Hohmann's transfer* is the most economical manoeuvre, but it is also the one that costs more in terms of time. Because of the long time required for this manoeuvre, it is not convenient if there is a crew on board.

Here is the calculation about the time taken to complete the maneuver:

$$\Delta T_H = \frac{T_E}{2} = \pi\sqrt{\frac{a_H^3}{\mu}} \tag{3.106}$$

It is corresponding to half the orbital period of the transfer orbit.

In order to reduce t, are used more expensive trajectories like parabolic or hyperbolic. Starting tangent to perigee $\rightarrow \varphi = 0$ (*fight path angle*), and arriving at the final orbit by travelling a shorter distance with higher speed:

$$\Delta V_1 > \Delta V_{1H} \tag{3.107}$$

To deorbit a debris, it is necessary to give it a certain impulsive ΔV, reducing the perigee of the orbit. The manoeuvre is carried out at the apogee of the elliptical orbit of the debris. Therefore the Hohmann transfer formulas (circular orbits) needs some variations. Since the apogee of the elliptical orbit of the debris coincides with the apogee of the Hohmann orbit, it will be enough to give only one impulse to vary the velocity. The energy is conserved. Therefore it can be written:

$$E_d = \frac{V_a^2}{2} - \frac{\mu}{r_a} = -\frac{\mu}{2a} \quad \Rightarrow \quad V_a = \sqrt{2\mu\Big(\frac{1}{r_a} - \frac{1}{2a}\Big)} \tag{3.108}$$

$$E_H = \frac{V_H^2}{2} - \frac{\mu}{r_a} = -\frac{\mu}{r_a + r_p^*} \quad \Rightarrow \quad V_H = \sqrt{2\mu\Big(\frac{1}{r_a} - \frac{1}{r_a + r_p^*}\Big)} \tag{3.109}$$

Where: E_d is the debris's Mechanical energy on his orbit and r_p^* is the perigee of the final orbit ($r_p^* = r_E$). Change in velocity to deorbit the debris is:

$$\Delta V_{deo} = \left|\sqrt{2\mu\Big(\frac{1}{r_a} - \frac{1}{2a}\Big)} - \sqrt{2\mu\Big(\frac{1}{r_a} - \frac{1}{r_a + r_p^*}\Big)}\right| \tag{3.110}$$

3.4 Mass estimation

The mass of the deorbiting kit m_k is given by the sum of two contributions, the propellant m_p and the structure m_s:

$$m_k = m_p + m_s \tag{3.111}$$

Where the mass of the structures can be approximated as proportional to the mass of propellant:

$$m_s = \epsilon m_p \tag{3.112}$$

In order to proceed with the calculation, *Tsiolkovsky rocket equation*, which describes the motion of veichles that follow the basic principle of a rocket, is introduced:

$$m_f = m_0 e^{-\Delta V_{deo}/C_k} \tag{3.113}$$

And introduce the final mass after the manoeuvre m_f, initial mass m_0, effective exhaust velocity $c_k = g_0 I_{sp}$ of deorbiting kit.

$$m_p = m_0 - m_f = m_0\Big(1 - e^{-\Delta V_{deo}/C_k}\Big) \tag{3.114}$$

Knowing that the mass of the debris is m_D:

$$m_D + m_s = (m_D + m_s + m_p)e^{-\Delta V_{deo}/C_k} \tag{3.115}$$

Assuming $e^{-\Delta V_{deo}/C_k} = \phi$:

$$m_D + m_s = (m_D + m_s + m_p)\phi \tag{3.116}$$

$$m_D + m_s = (m_D + m_k)\phi \tag{3.117}$$

$$m_k\phi = m_D + m_s - m_D\phi \tag{3.118}$$

$$m_k\phi = m_D + \epsilon m_p - m_D\phi \tag{3.119}$$

And considering:

$$m_p = m_0(1-\phi) = (m_D + m_k)(1-\phi) \tag{3.120}$$

It can be obtained:

$$m_k = \frac{m_D}{\phi} + \frac{\epsilon}{\phi}(m_D + m_k)(1-\phi) - m_D \tag{3.121}$$

$$m_k\left(1-\frac{\epsilon}{\phi}(1-\phi)\right)=\frac{m_D+\epsilon m_D(1-\phi)-m_D\phi}{\phi} \tag{3.122}$$

Obtaining the final expression of deorbiting kit mass:

$$m_k=\frac{m_D(1+\epsilon)(1-\phi)}{1-(1+\epsilon)(1-\phi)} \tag{3.123}$$

In addition, in order to calculate the propellant consumption of the chaser, it is necessary to start from the final mass of the mission, which is known because it is equal to the dry mass of the chaser (deorbiting kits already delivered and all transfers completed). Then we proceed backwards. We consider $i = 1, 2, n_{leg}$ where n_{leg} is the number of transfers to be made. Once the "i" leg (transfer) with mass $(m_f)_i$ is completed, the de-orbiting kit is issued to the "$i+1$" debris, from which the "$i+1$" leg with mass $(m_0)_{i+1}$ will start. Therefore:

$$(m_f)_i=(m_0)_{i+1}+(m_k)_{i+1} \tag{3.124}$$

And for the last debris: $(m_0)_{n_{leg}+1}=m_d$.
Initial mass of "i" leg can be found through equation 3.113:

$$(m_0)_i=\frac{(m_f)_i}{e^{-\Delta V_i/C_c}} \tag{3.125}$$

Obtaining the fuel consumption of the chaser on the "i" leg:

$$(m_p)_i=(m_0)_i-(m_f)_i=(m_f)_i\left(\frac{1-e^{-\Delta V_i/C_c}}{e^{-\Delta V_i/C_c}}\right) \tag{3.126}$$

So $m_{start}=(m_0)_1+(m_k)_1$ can be obtained going backwards.

Chapter 4

Mission and code

4.1 General explanation

The mission consists of removing a sequence of four debris orbiting around the Earth. The debris in question comes from Russian Kosmos 3M launchers, a two-stage rocket that has been in use since 15 May 1967. A total of 446 launches have been carried out, of which 22 have failed. Space debris from these rockets can be identified in two different clusters at an orbital inclination of 74° (120 debris) and 82° (155 debris). You can see from image 4.1 the distribution of debris as a function of the semi-major axis a and longitude of the ascending node Ω (RAAN).

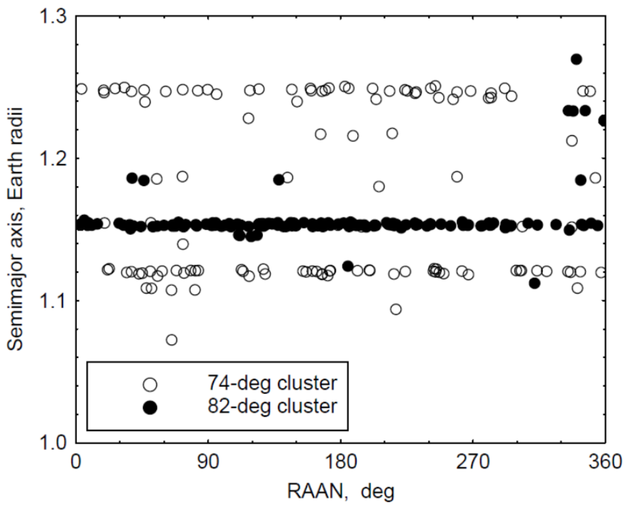

Figure 4.1: Debris groupings at 74° and 82°.

For this thesis, the grouping located at an inclination of about 74° was chosen. In this mission is considered that the spacecraft is already on the first debris at

$t = 0$. After the time necessary to apply the de-orbiting kit t_{DT} has passed, the spacecraft makes the transfer to the second debris, where it applies the kit during t_{DT} and so on until the fourth debris.

As can be imagined, having 120 debris, the possible combinations are very high. For this reason and not to have a redundant amount of results, constraints are also imposed on the total ΔV and single ΔV of each leg. The developed computational code calculates all possible sequences, calculates their cost in terms of ΔV and selects the most convenient ones that fall within the time and ΔV requirements. The possible combinations would be:

$$120^4 = 207360000 \tag{4.1}$$

Of course, some sequences repeat, and eliminating them results in the following:

$$\frac{120!}{(120-4)!} = 197149680 \tag{4.2}$$

The constraints imposed are:

- $\Delta V_{tot} = \Delta V_{leg1} + \Delta V_{leg2} + \Delta V_{leg3} < 0.75 \quad \frac{km}{s}$
- $\Delta V_{leg} < 0.3 \quad \frac{km}{s}$

Thanks to these two constraints and the constrain on time, a much smaller number of possible solutions (about 3800) is found.

4.2 Transfers

The most favourable conditions occur when the two debris are coplanar, that is, when Δi equals zero (all debris are at $i = 74°$), and $\Delta\Omega$ equals zero. As the difference in longitude of the ascending node of the chaser and the target increases, the cost in terms of ΔV and time will also increase. So, as mentioned in chapter 3, Hohmann's transfer theory is used for the transfer manoeuvre between two debris. From the paragraph 3.2 it can be seen that due to the orbital perturbations caused by the Earth's oblateness, the longitude of the ascending node varies in time. This effect is exploited to decrease the costs under certain conditions.

In this thesis, a new strategy (Fixed time-Strategy) is implemented, which looks for an optimal transfer time in order to speed up the mission. In our case, if the next debris is not reached with Hohmann's transfer in a given time, the j_2 perturbation that modifies the omega will be used: debris with different orbital parameters will have a different RAAN variation. We, therefore, impose a maximum time ($t_{max} = 30$ days) for the duration of the transfer of 30 days, and the transfer is carried out.

4.2.1 Optimal time-Strategy

Optimal time-strategy looks for the optimal encounter time t_{opt} between chaser and target for which $\Delta\Omega = 0$ and can be written as:

$$\Omega_k(t_0) + t_{opt}\dot{\Omega}_k = \Omega_{k+1}(t_0) + t_{opt}\dot{\Omega}_{k+1} + 2K\pi \tag{4.3}$$

$$t_{opt} = \frac{\Omega_{k+1}(t_0) - \Omega_k(t_0) + 2K\pi}{\dot{\Omega}_k - \dot{\Omega}_{k+1}} \tag{4.4}$$

Where K is an arbitrary constant chosen in order to obtain the minimum positive encounter time, t_{opt} is the time required for complanarity between debris "k" and "$k+1$" to occur, Ω_k and Ω_{k+1} are longitude of ascending nodes, $\dot{\Omega}_k$ and $\dot{\Omega}_{k+1}$ are the variations in time of Ω.

After calculating the optimal encounter time under coplanar conditions, the cost in terms of ΔV is calculated:

$$\Delta V = \frac{1}{2}\sqrt{\frac{1}{a_{min}}}\sqrt{\left(\frac{\Delta a}{a}\right)^2 + (\Delta e)^2} \tag{4.5}$$

Which takes into account the difference in eccentricity and semi-major axis between the two debris.
Δe can be obtained by varying the argument of perigee:

$$\omega_{k(opt)} = \omega_k + \dot{\omega}_k t_{opt} \tag{4.6}$$

$$\omega_{k+1(opt)} = \omega_{k+1} + \dot{\omega}_{k+1} t_{opt} \tag{4.7}$$

For reasons of space and more clarity, the debris "k" and "$k+1$" may be called "i" and "j" respectively, while the terms marked with an asterisk means that they are those associated with optimal time $t_{opt} = t^*$ ($\omega_{k(opt)} = \omega_i^*$, $\omega_{k+1(opt)} = \omega_j^*$).

$$(\Delta e)^2 = [e_i \cos(\omega_i^*) - e_j \cos(\omega_j^*)]^2 + [e_i \sin(\omega_i^*) - e_j \sin(\omega_j^*)]^2 \tag{4.8}$$

As mentioned above, when the spacecraft arrives on a debris, it must spend the service time t_{DT} to install the de-orbiting kit. If the optimal time t^* for the transfer is less than the service time, it is necessary to wait for the coplanarity condition to be restored. So:

$$\Delta t_w = \left| \frac{2\pi}{\dot{\Omega}_i - \dot{\Omega}_j} \right| \tag{4.9}$$

So if $t_{DT} < t^*$ the transfer is carried out normally, while if $t_{DT} > t^*$ the situation in which $\Delta\Omega = 0$ is expected to occur again. We are now at t_{DT}, calculate the wait period:

$$n_{per} = int\left[\frac{|(t_{DT} - t^*)|}{\Delta t_w}\right] \tag{4.10}$$

Where *int* extracts the integer part.
And the encounter time at which the first successive coplanarity will occur is obtained:

$$t^{'*} = t^* + (n_{per} + 1)\Delta t_w \tag{4.11}$$

Now make the first impulsive transfer and reach the second debris, on which you will wait for the service time for the application of the de-orbiting kit and proceed with this procedure until the fourth debris.
The moment the fourth debris is reached, the mission is considered to be completed. The cost of the mission can then be calculated in terms of ΔV:

$$\Delta V_{tot} = \Delta V_1 + \Delta V_2 + \Delta V_3 \tag{4.12}$$

As mentioned above, if the time requirements are not met in any of the individual trips, i.e. the coplanarity situation is not reached in the stipulated time (30 days), Fixed time-Strategy is used.

4.2.2 Fixed time-Strategy

As better described in [19], this strategy assumes a situation where the two debris do not reach coplanarity in the expected time:

- *Longitude of the ascending node* $\rightarrow \quad \Delta\Omega_{k+1} - \Delta\Omega_k \neq 0$
- *Semi-major axis* $\rightarrow \quad a_{k+1} - a_k \neq 0$
- *Orbital inclination* $\rightarrow \quad i_{k+1} - i_k \neq 0$

As can be seen from the assumptions, this strategy can also work for debris with different orbital inclinations i. The Ω difference, since it varies in time, is understood to be at the time (t_{max}) the manoeuvre is performed.
In order to take into account the changes of Ω, a and i, we introduce the quantities

x, y, z. The strategy under consideration is a two-impulse transfer: both partially change quantities x, y, z.

$$x = \Big(\Omega_{k+1}(t_{max}) - \Omega_k(t_{max})\Big) \sin i_0 \nu_0 \tag{4.13}$$

$$y = \frac{a_{k+1} - a_k}{2a_0} \nu_0 \tag{4.14}$$

$$z = (i_{k+1} - i_k)\nu_0 \tag{4.15}$$

Where:

$$\Omega_{k+1}(t_{max}) = \Omega_{k+1} + \dot{\Omega}_{k+1} t_{max} \tag{4.16}$$

$$\Omega_k(t_{max}) = \Omega_k + \dot{\Omega}_k t_{max} \tag{4.17}$$

$$a_0 = \frac{(a_{k+1} + a_k)}{2} \tag{4.18}$$

$$i_0 = \frac{(i_{k+1} + i_k)}{2} \tag{4.19}$$

$$\nu_0 = \sqrt{\frac{\mu}{a_0}} \tag{4.20}$$

The first impulse ΔV_a is:

$$\Delta V_a = \sqrt{\Big(s_x x\Big)^2 + \Big(s_y y\Big)^2 + \Big(s_z z\Big)^2} \tag{4.21}$$

s_x, s_y and s_z are coefficients respectively of x, y, z have no constraints and can be positive, negative, smaller or larger than unity.
By differentiating equation 3.66 it can be seen that small variations in the semi-major axis and orbital inclination cause a change in the RAAN ratio, so in addition, there is a change in Ω due to the first impulse during the transfer time:

$$\Delta x = -m s_y y - n s_z z \tag{4.22}$$

This effect is added to the effect of the impulses and coefficients m and n are written as:

$$m = (7\dot{\Omega}_0) \sin i_0 t \tag{4.23}$$

$$n = (\dot{\Omega}_0 \tan i_0) \sin i_0 t \tag{4.24}$$

Where $\dot{\Omega}_0$ is the average RAAN rate of the chaser and the target:

$$\dot{\Omega}_0 = \frac{(\dot{\Omega}_{k+1} + \dot{\Omega}_k)}{2} \tag{4.25}$$

Proceeding, the second impulse is written as:

$$\Delta V_b = \sqrt{\left(x - s_x x - \Delta x\right)^2 + \left(y - s_y y\right)^2 + \left(z - s_z z\right)^2} \tag{4.26}$$

Obtaining finally the total $\Delta V_{tot} = \Delta V_a + \Delta V_b$:

$$\Delta V_{tot} = \sqrt{\left(s_x x\right)^2 + \left(s_y y\right)^2 + \left(s_z z\right)^2} + \sqrt{\left(x - s_x x - \Delta x\right)^2 + \left(y - s_y y\right)^2 + \left(z - s_z z\right)^2} \tag{4.27}$$

The variables s_x, s_y. and s_z are still unknown; in order to find the minimum value of ΔV_{tot}, "classical Minimum inclination maneuvers" are exploited.[20] After some mathematical work, the coefficients can be derived:

$$s_x x = \frac{2x + my + nz}{\left(4 + m^2 + n^2\right)} \tag{4.28}$$

$$s_y y = -\frac{2mx - \left(4 + n^2\right)y + mnz}{\left(8 + 2m^2 + 2n^2\right)} \tag{4.29}$$

$$s_z z = -\frac{2nx - \left(4 + m^2\right)z + mny}{\left(8 + 2m^2 + 2n^2\right)} \tag{4.30}$$

By substituting equations 4.28, 4.29, 4.30 into equation 4.27, the minimum ΔV_{tot} can be approximated. Note that if x, y or z are equal to zero, the coefficients s_x, s_y, s_z might not be defined.
To evaluate the cost of changing raan, an important observation can be made in the solution estimated using s_x, s_y, s_z:

$$s_x x = x - s_x x - \Delta x \tag{4.31}$$

It can be seen that the two impulses provide the exact change in $\Delta\Omega$. Equation 4.31 can be substituted into equation 4.26 to simplify the expression. You can see, by substituting equation 4.28 into equation 4.29 and 4.30 that, in the case where s_x is zero, both s_y and s_z are 1/2. Therefore equation 4.31 implies that if $s_x = 0$, $x = \Delta x$, which means that RAAN is not controlled by thrust but rather matched by using only the perturbation effect provided by the changes on inclination and semi-major axis.[19]

Another expression is provided that also accounts for the additional cost of eccentricity change:

$$\Delta V'_{tot} = \sqrt{\Delta V_a^2 + \left(\frac{1}{2}\Delta V_e\right)^2} + \sqrt{\Delta V_b^2 + \left(\frac{1}{2}\Delta V_e\right)^2} \tag{4.32}$$

Where the velocity change ΔV_e is given by:

$$\Delta V_e = \frac{1}{2}\nu_0\sqrt{\Delta e_y^2 + \Delta e_x^2} \tag{4.33}$$

Note that is intended for small variations of eccentricity and $e_y = e \sin\omega$, $e_x = e\cos\omega$ (non-singular equinoctial elements). As can be seen from the expression, the ΔV change for the eccentricity variation is divided equally between the two impulses and is perpendicular to ΔV_a and ΔV_b. Then through the equation 4.32, the variation of eccentricity is implemented in the formula of ΔV_{tot} (equation 4.27).

As mentioned above, this strategy is used if the coplanarity situation is not reached in the set time. So for each leg, the code chooses whether to use Optimal time-Strategy or Fixed time-Strategy.

4.3 Deorbiting

There are several methods to remove a debris, as described in the chapter 2.2 In this thesis the re-entry method using a de-orbiting kit is used, which means that the de-orbiting kit that is installed on the debris is used to impose an impulse that serves to decrease the perigee of the orbit. As the perigee of the orbit decreases, it moves closer and closer to the atmosphere until the debris is burnt by thermal forces and mechanical loads due to the increasing density of the atmosphere. In this case, the braking action of the atmospheric resistance tends to reduce further the required ΔV_{deo}, but this contribution is not counted in this thesis. The calculations about de-orbiting are explained in section 3.3.1.

Chapter 5

Results

The last part of this thesis will focus on explaining the results obtained from the FORTRAN code.

The two possible strategies are recalled:

Optimal time-Strategy : Once the encounter time has been found using the formulas given in section 4.2.1, the maximum time for reaching coplanarity is set. If it is respected, the transfer between coplanar orbits is carried out.

Fixed time-Strategy : This strategy is used for legs where the coplanarity is not reached in the predefined time, in this case, the transfer is completed in the maximum time even if the orbits are not coplanar, so as already mentioned, we have: $\Delta\Omega_i \neq \Delta\Omega_j$, $\Delta i_i \neq \Delta i_j$, $\Delta a_i \neq \Delta a_j$. Two pulses are then imposed, one initial and one final (to compensate the first) to move to the next debris.

As already mentioned in section 4, the code selects all sequences that fall within the predefined parameters.

5.1 Input file and input data

The code receives as input a text file containing all debris data. Part of the file is shown below:

5730	57754	1.139622722	0.0703004	73.8955	72.88907533	347.1164732	329.6363069
7004	57754	1.072198598	0.0193358	73.9374	65.24650994	338.5901652	302.4392283
12983	57754	1.246442609	0.0114184	73.9842	259.2125865	305.7766071	253.6394642
7831	57754	1.24913198	0.0130198	73.9846	185.6173314	334.8919514	53.20034061
20557	57754	1.247552564	0.0151519	73.9861	118.4929601	43.30712578	322.580505
3819	57754	1.186064398	0.0010416	73.9879	353.3878932	112.6116537	212.5467737
12115	57754	1.228078054	0.0020243	73.9917	117.4966021	109.2759557	356.3336141
16457	57754	1.249175607	0.0134056	73.9952	291.64356	52.25212629	159.509681
14619	57754	1.246381761	0.0126987	73.9959	231.3966092	318.8134199	170.1803433
8897	57754	1.248977341	0.012566	73.9974	159.4952186	110.5290547	228.3390947
5181	57754	1.185362417	0.0055545	73.9979	55.09241263	240.2593641	306.6923296
7686	57754	1.2490041	0.0164985	73.9995	201.8422888	152.7048411	6.16522549
13649	57754	1.12045574	0.0019563	73.9995	320.106496	155.3244034	221.9556167
21984	57754	1.248179465	0.0123747	74.0014	89.64630118	82.99066964	273.7885414
13386	57754	1.248954054	0.0154049	74.0018	26.7795538	29.99383705	161.8153013
4579	57754	1.108517607	0.0011701	74.003	51.53706009	105.9450972	275.7224873
13769	57754	1.248774331	0.013597	74.0041	3.881133645	289.6939108	259.6257055
18121	57754	1.247969575	0.0130993	74.0049	223.8707691	14.36952346	185.7211515
3048	57754	1.108694632	0.0006129	74.0061	341.0956907	219.183189	326.6523103
18945	57754	1.246981193	0.013933	74.0069	167.4406013	353.9455166	217.9022922
16766	57754	1.247280795	0.0133889	74.0071	225.4840978	164.9293082	350.7035872
19910	57754	1.247456596	0.0132743	74.0076	160.0677555	195.1881399	72.56485074
18586	57754	1.120607581	0.0019849	74.0088	243.0952984	340.944055	317.4396687
6853	57754	1.24358211	0.0086824	74.009	296.3198579	162.8575711	328.145623
11883	57754	1.247024342	0.0133184	74.0106	349.7179436	306.065639	313.2250388
8295	57754	1.248254434	0.0126235	74.0111	146.8586765	28.2831587	135.0923603
17146	57754	1.247221365	0.0123413	74.0115	213.4065384	28.08416055	158.2035088
2802	57754	1.117055472	0.0066901	74.0121	117.8029928	211.5577655	334.451729
11699	57754	1.247912554	0.0142111	74.0126	46.4689809	131.9844318	83.31983277
16953	57754	1.120348293	0.001356	74.0129	224.0221072	125.3464636	309.1451123
9598	57754	1.246874773	0.013736	74.0131	61.19847233	221.1817093	320.6904493
11136	57754	1.250251195	0.0129749	74.0136	182.9220282	3.788026607	278.8447211
15006	57754	1.247180356	0.0133509	74.0138	268.5521924	179.5050611	229.4047694
4255	57754	1.180074896	0.0011344	74.0142	206.1684692	76.985661	68.27956769
6320	57754	1.212260654	0.0023925	74.0152	337.4132156	50.89314115	333.4874908
11427	57754	1.12032488	0.0021078	74.0167	334.7397613	153.8381605	53.83211726
6683	57754	1.241462054	0.007194	74.0182	204.1966134	192.2273025	61.60278399
6125	57754	1.242295355	0.0069795	74.0184	280.7548887	167.4162638	359.3946507
14179	57754	1.245597583	0.012973	74.0195	230.7491682	350.4803833	171.5880572
5555	57754	1.244979263	0.007584	74.0196	95.73392194	258.7564886	322.9226738
6020	57754	1.151803884	0.0021721	74.0196	194.2318781	190.5300289	44.62608856
6826	57754	1.216852788	0.0028655	74.0196	166.5243203	57.72388111	72.99273776
11546	57754	1.248128763	0.0125826	74.0197	72.71196154	298.9723995	139.8910266
5239	57754	1.15456756	0.0010528	74.0216	51.14257917	25.33145126	192.5700696

Figure 5.1: Extract of input text file.

In order in the file it shows:

- NORAD identify number of debris, in this thesis called with numbers from 1 to 120.
- Epoch, i.e. the reference time of the mission: 1 January 2017 00:00 UT.
- Semi-major axis a.
- Eccentricity e.
- Orbital inclination i [°].

- Longitude of the ascending node Ω [°].
- Argument of periapsis ω [°].
- Mean anomaly M [°].

The following is a list of all the parameters used and inserted into the code to obtain the results:

- Earth's radius $\rightarrow$ r_E=6378.1363 km.
- Standard gravitational parameter $\rightarrow$ μ_E =3968600.4415 km^3/s^2.
- Reference speed $\rightarrow$ $V_{ref} = \frac{\mu_E}{r_E}$ =7.9353 km/s.
- Reference time $\rightarrow$ $t_{ref} = \frac{r_E}{V_{ref}}$ =806.8177 s.
- Specific impulse of chaser and deorbiting kit $\rightarrow$ I_{sp} =310 s.
- Dry mass of the chaser $\rightarrow$ m_d=2000 kg.
- Mass of the debris $\rightarrow$ m_d =1450 kg.
- $\epsilon = \frac{m_s}{m_p}$ =0.1 .
- Service time, the time taken by the spacecraft to install the deorbiting kit $\rightarrow$ DT =10 days.
- Maximum duration of transfer $\rightarrow$ t_{max} =30 days.
- Maximum cost in speed impulse $\rightarrow$ ΔV_{tot} <0.75 km/s.
- Maximum cost in speed impulse $\rightarrow$ ΔV_{leg} <0.3 km/s.

For ease of use in the charts and tables, the Optimal time-Strategy will be called 0-Strategy, and the Fixed time-Strategy will be called 1-Strategy.

After this summary of the data entered in the code, an extrapolation of the most important results obtained follows.

All results were grouped in an excell file like in the image that follows:

3841 sequences with dVtot<0,75 e dVleg<0,3															
	sequence				strategy			deltaV				times			
index	i1	i2	i3	i4	leg1	leg2	leg3	tot	leg1	leg2	leg3	start	arrival at i2	arrival at i3	arrival at i4
1	1	85	44	94	1	1	1	0,6948	0,21135	0,19717	0,28628	10	50	90	120
2	1	85	44	95	1	1	0	0,56865	0,21135	0,19717	0,16013	10	50	90	116,208
3	1	85	44	110	1	1	1	0,52819	0,21135	0,19717	0,11968	10	50	90	120
4	1	85	63	112	1	1	1	0,69444	0,21135	0,29206	0,19103	10	50	90	120
5	1	85	63	115	1	1	1	0,58211	0,21135	0,29206	0,0787	10	50	90	120
6	1	85	63	119	1	1	1	0,58864	0,21135	0,29206	0,08523	10	50	90	120
7	1	85	95	44	1	1	0	0,61068	0,21135	0,2392	0,16013	10	50	90	116,208
8	1	85	95	94	1	1	1	0,63883	0,21135	0,2392	0,18828	10	50	90	120
9	1	85	95	110	1	1	0	0,49228	0,21135	0,2392	0,04173	10	50	90	103,9588
10	1	85	95	114	1	1	1	0,74664	0,21135	0,2392	0,2961	10	50	90	120
11	1	85	110	44	1	1	1	0,4844	0,21135	0,15338	0,11968	10	50	90	120
12	1	85	110	94	1	1	1	0,54739	0,21135	0,15338	0,18267	10	50	90	120
13	1	85	110	95	1	1	0	0,40646	0,21135	0,15338	0,04173	10	50	90	103,9588
14	1	85	110	114	1	1	1	0,65737	0,21135	0,15338	0,29264	10	50	90	120
15	1	94	11	15	1	0	1	0,54932	0,12983	0,21574	0,20376	10	50	81,87259	111,8726
16	1	94	11	98	1	0	0	0,55109	0,12983	0,21574	0,20552	10	50	81,87259	84,69706
17	1	94	11	100	1	0	0	0,56122	0,12983	0,21574	0,21566	10	50	81,87259	88,12916
18	1	94	11	114	1	0	0	0,56165	0,12983	0,21574	0,21609	10	50	81,87259	82,16892
19	1	94	95	44	1	1	0	0,37397	0,12983	0,08401	0,16013	10	50	90	116,208
20	1	94	95	85	1	1	1	0,34848	0,12983	0,08401	0,13464	10	50	90	120
21	1	94	95	110	1	1	0	0,25557	0,12983	0,08401	0,04173	10	50	90	103,9588
22	1	94	95	114	1	1	1	0,50993	0,12983	0,08401	0,2961	10	50	90	120
23	1	94	100	11	1	1	1	0,55106	0,12983	0,17393	0,2473	10	50	90	120

Figure 5.2: Example of excell table - selected sequences.

As mentioned above, the sequences selected by the code that respect the imposed constraints are **3841**, in the image:

- *Index* → Given simply to distinguish sequences from each other.
- *i1, i2, i3, i4* → The number of the debris, the code receives an identification number of the debris, for simplicity in this thesis work the debris is distinguished with a number ranging from 1 to 120.
- *leg1, leg2, leg3* → The strategy used in each leg, maybe 0 or 1.
- *deltaV* → The speed impulse provided: total impulse followed by the impulse of the individual transfers.
- *Times* → The total time taken to complete the mission followed by the time taken to depart from the debris (the service time required to apply the kit is also counted).

Of all the sequences, the most critical sequences were selected, i.e. those with a low ΔV, as can be seen in figure 5.2 (highlighted line).
Three different strategies were used in the original code. The data obtained from this thesis work was compared with the results obtained from the original code and the results obtained using a non-approximated code, which however requires a much higher computational cost.

The strategies used in the original calculation code are:

Strategy 1 : It corresponds to Optimal time-strategy used in this thesis.

Strategy 2 : If the encounter time does not fall within the permitted time window, it is possible to conclude the transfer by waiting a time equal to the maximum duration (t_{max} =30 days), to reduce as much as possible the $\Delta\Omega$ separating the debris, and finally perform the $\Delta\Omega$ change, orbital inclination change and semi-major axis change in a single manoeuvre.

Strategy 3 : If the meeting time is not within the allowed time window (t_{max} =30 days), it is possible to change the semi-major axis so as to vary the influence of J_2 on $\dot{\Omega}$ which therefore allows reaching $\Delta\Omega$=0 condition between the two debris. Then returning to the starting semi-axis through a new impulsive manoeuvre and finally perform the classic transfer between coplanar orbits since the encounter has been achieved.

Using the same constraints but with the strategies of the original code, 983 possible sequences were selected. It can therefore be said that this strategy provides more mission scenarios.

5.2 Results

Table 5.1 contains all possible solutions using only the Optimal time-strategy, i.e. in the case where coplanarity between orbits is reached in the predefined time and the easiest manoeuvre can be performed.

Fifty-seven sequences were obtained using only the Optimal time-strategy, which is only 1.5% of the total number of sequences obtained. In graph 5.3 it can be seen that in some cases, the third transfer is completed in less than 60 days in total, which means that the debris selected by the code for these sequences are in positions very close to each other. By very close, we mean a slight difference in the semi-major axis, orbiting at an orbital inclination of 74° and reaching coplanar condition $\Delta\Omega = 0$ in a concise amount of time.

	sequence				**strategy**			ΔV **[km/s]**				**times [days]**			
index	i1	i2	i3	i4	leg1	leg2	leg3	tot	leg1	leg2	leg3	start	arr. at i2	arr. at i3	arr. at i4
159	2	115	44	46	0	0	0	0,59674	0,18659	0,11346	0,2967	10	30,24888	52,24024	81,84215
160	2	115	44	63	0	0	0	0,46053	0,18659	0,11346	0,16048	10	30,24888	52,24024	53,65829
204	4	71	32	34	0	0	0	0,4395	0,10728	0,11131	0,22091	10	34,45748	54,47393	82,75217
229	11	63	44	46	0	0	0	0,72278	0,26561	0,16048	0,2967	10	34,77001	63,65829	81,84215
261	11	115	44	46	0	0	0	0,62646	0,21631	0,11346	0,2967	10	21,10573	52,24024	81,84215
262	11	115	44	63	0	0	0	0,49025	0,21631	0,11346	0,16048	10	21,10573	52,24024	53,65829
381	16	112	2	57	0	0	0	0,4123	0,04118	0,1855	0,18562	10	21,36667	55,04105	71,82285
382	16	112	2	73	0	0	0	0,3747	0,04118	0,1855	0,14802	10	21,36667	55,04105	68,32462
383	16	112	2	83	0	0	0	0,40863	0,04118	0,1855	0,18195	10	21,36667	55,04105	63,72641
555	29	11	95	110	0	0	0	0,50779	0,20021	0,26585	0,04173	10	44,46306	74,75348	103,9588
567	29	51	11	66	0	0	0	0,41325	0,05162	0,16678	0,19484	10	28,5211	46,52599	68,98823
569	29	51	11	94	0	0	0	0,43414	0,05162	0,16678	0,21574	10	28,5211	46,52599	71,87259
570	29	51	11	95	0	0	0	0,48426	0,05162	0,16678	0,26585	10	28,5211	46,52599	64,75348
572	29	51	11	110	0	0	0	0,44002	0,05162	0,16678	0,22162	10	28,5211	46,52599	56,17571
612	41	71	32	34	0	0	0	0,53679	0,20457	0,11131	0,22091	10	29,54496	54,47393	82,75217
707	44	51	11	66	0	0	0	0,63433	0,27271	0,16678	0,19484	10	21,34172	46,52599	68,98823
709	44	51	11	94	0	0	0	0,65523	0,27271	0,16678	0,21574	10	21,34172	46,52599	71,87259
710	44	51	11	95	0	0	0	0,70534	0,27271	0,16678	0,26585	10	21,34172	46,52599	64,75348
712	44	51	11	110	0	0	0	0,66111	0,27271	0,16678	0,22162	10	21,34172	46,52599	56,17571
723	44	66	11	98	0	0	0	0,69902	0,29865	0,19484	0,20552	10	43,61654	78,98823	84,69706
724	44	66	11	100	0	0	0	0,70915	0,29865	0,19484	0,21566	10	43,61654	78,98823	88,12916
725	44	66	11	114	0	0	0	0,70958	0,29865	0,19484	0,21609	10	43,61654	78,98823	82,16892
904	51	11	95	110	0	0	0	0,47436	0,16678	0,26585	0,04173	10	46,52599	74,75348	103,9588
918	51	29	11	66	0	0	0	0,44668	0,05162	0,20021	0,19484	10	28,5211	44,46306	68,98823
920	51	29	11	94	0	0	0	0,46757	0,05162	0,20021	0,21574	10	28,5211	44,46306	71,87259
921	51	29	11	95	0	0	0	0,51768	0,05162	0,20021	0,26585	10	28,5211	44,46306	64,75348
923	51	29	11	110	0	0	0	0,47345	0,05162	0,20021	0,22162	10	28,5211	44,46306	56,17571
931	51	44	115	63	0	0	0	0,43179	0,27271	0,11346	0,04563	10	21,34172	52,24024	78,51494
1134	58	60	48	102	0	0	0	0,66119	0,28441	0,28684	0,08994	10	28,25352	53,52121	79,43521
1135	58	60	48	104	0	0	0	0,7437	0,28441	0,28684	0,17245	10	28,25352	53,52121	56,27167
1143	58	104	60	48	0	0	0	0,56395	0,16775	0,10935	0,28684	10	22,18809	36,30368	43,52121
1151	60	104	48	102	0	0	0	0,37175	0,10935	0,17245	0,08994	10	36,30368	66,27167	79,43521
1153	60	104	102	48	0	0	0	0,40503	0,10935	0,20573	0,08994	10	36,30368	69,10153	79,43521
1180	61	94	95	1	0	0	0	0,55458	0,22056	0,04665	0,28737	10	26,47582	46,51473	54,78957
1181	61	94	95	11	0	0	0	0,53306	0,22056	0,04665	0,26585	10	26,47582	46,51473	64,75348
1205	61	95	94	1	0	0	0	0,59062	0,27107	0,04665	0,27291	10	30,39911	46,51473	76,29329
1206	61	95	94	11	0	0	0	0,53345	0,27107	0,04665	0,21574	10	30,39911	46,51473	71,87259
1330	63	11	95	110	0	0	0	0,57319	0,26561	0,26585	0,04173	10	34,77001	74,75348	103,9588
1443	66	44	63	115	0	0	0	0,50477	0,29865	0,16048	0,04563	10	43,61654	63,65829	78,51494
1797	79	41	69	88	0	0	0	0,39859	0,10176	0,2007	0,09613	10	43,4662	80,97205	106,2532
2170	88	41	69	79	0	0	0	0,40077	0,10347	0,2007	0,0966	10	44,89441	80,97205	107,0303
2433	94	95	11	98	0	0	0	0,51802	0,04665	0,26585	0,20552	10	46,51473	74,75348	84,69706
2434	94	95	11	100	0	0	0	0,52815	0,04665	0,26585	0,21566	10	46,51473	74,75348	88,12916
2435	94	95	11	114	0	0	0	0,52858	0,04665	0,26585	0,21609	10	46,51473	74,75348	82,16892
2519	95	94	11	98	0	0	0	0,46791	0,04665	0,21574	0,20552	10	46,51473	81,87259	84,69706
2520	95	94	11	100	0	0	0	0,47804	0,04665	0,21574	0,21566	10	46,51473	81,87259	88,12916
2521	95	94	11	114	0	0	0	0,47847	0,04665	0,21574	0,21609	10	46,51473	81,87259	82,16892
2879	104	60	48	102	0	0	0	0,48614	0,10935	0,28684	0,08994	10	36,30368	53,52121	79,43521
3395	115	2	16	83	0	0	0	0,37482	0,18659	0,15068	0,03755	10	30,24888	65,50958	93,78737
3430	115	11	63	44	0	0	0	0,6424	0,21631	0,26561	0,16048	10	21,10573	34,77001	53,65829
3491	116	60	48	102	0	0	0	0,49444	0,11766	0,28684	0,08994	10	28,94146	53,52121	79,43521
3492	116	60	48	104	0	0	0	0,57695	0,11766	0,28684	0,17245	10	28,94146	53,52121	56,27167
3497	116	104	48	102	0	0	0	0,49253	0,23014	0,17245	0,08994	10	32,38589	66,27167	79,43521
3623	119	2	16	83	0	0	0	0,36482	0,17659	0,15068	0,03755	10	41,14616	65,50958	93,78737
3685	119	44	63	115	0	0	0	0,33141	0,1253	0,16048	0,04563	10	33,16852	63,65829	78,51494
3686	119	44	66	11	0	0	0	0,6188	0,1253	0,29865	0,19484	10	33,16852	43,61654	68,98823
3690	119	44	115	63	0	0	0	0,28438	0,1253	0,11346	0,04563	10	33,16852	52,24024	78,51494

Table 5.1: Solutions using only Optimal time-strategy.

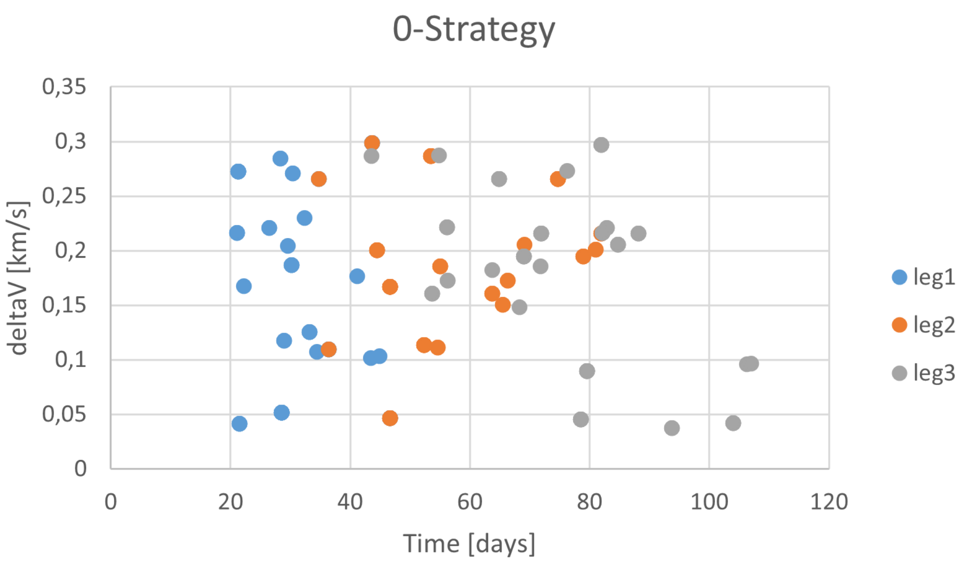

Figure 5.3: Sequences performed using only Optimal time-Strategy - ΔV function of time.

Graph 5.4 summarises only sequences that matched the selected sequences from the original code. They are extrapolated to compare them and check if they are convenient.

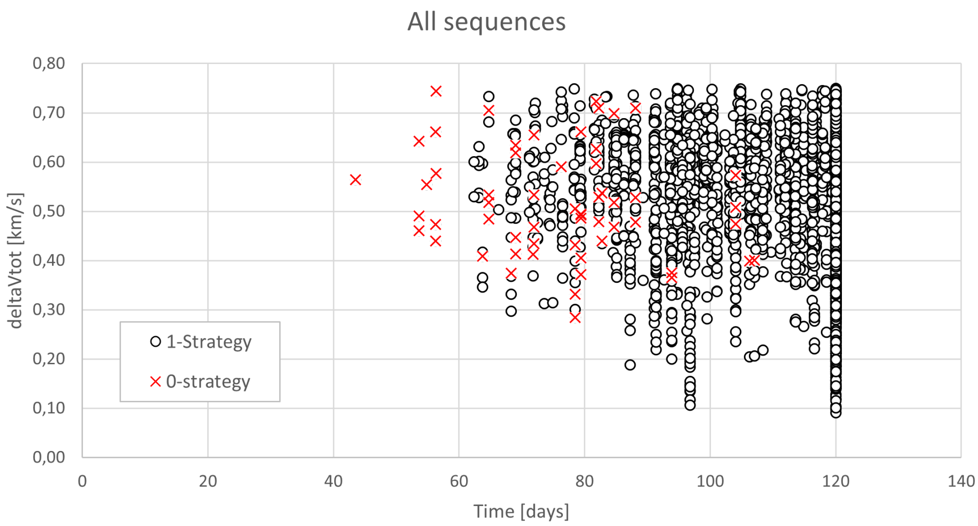

Figure 5.4: All sequences performed - ΔV function of time.

The following figure (5.5) shows all sequences obtained with the three comparing strategies (red crosses) and the results obtained in this thesis work (black circles). It was noted that the ΔV value of the sequence in the exam was always lower using the new strategy.

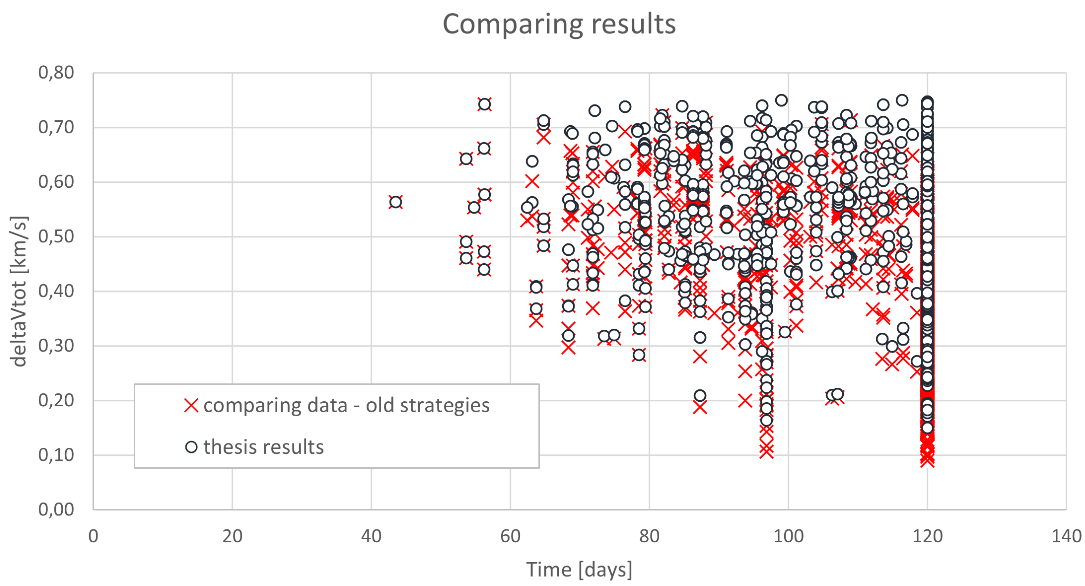

Figure 5.5: All sequences performed from old and new strategies - ΔV function of time.

Graph 5.6 represent the number of times the Fixed time or Optimal time-Strategy was used in the single transfer (leg).

It can be seen that the Optimal time-strategy is used about one-fourth of the times for each transfer. This is because, as already mentioned, it is challenging to achieve coplanarity in such a short period. It must be pointed out that the code is not programmed to optimise the distribution of strategies within a sequence according to the total time. It only chooses the strategy to be used if the time is within the constraint imposed or not for the single transfer.

That said, once the best sequences have been selected, it is possible to optimise the distribution of strategies by calculating, using other methods, a set of transfer constraints that allow a better distribution to be proposed. In other words, the results could be further improved by knowing the encounter times and the coplanarity situation between the debris a priori and by choosing the time constraints for each trip appropriately. This would also optimise the distribution of strategies within a sequence according to the total time.

As regards the results obtained by the original code, it was noticed that when strategy 2 or 3 was selected (coplanarity not reached within the imposed time constraints), many sequences were discarded at the second leg due to the imposed ΔV constraints (strategies 2 and 3 cost more in terms of ΔV and time). Those that were within the constraints mainly used Strategy 1 as it costs less and takes less time. This explains the rarity of sequences 1,1,1.

In this thesis, it has been noted that using the Fixed time-Strategy, the costs in terms of ΔV are often lower.

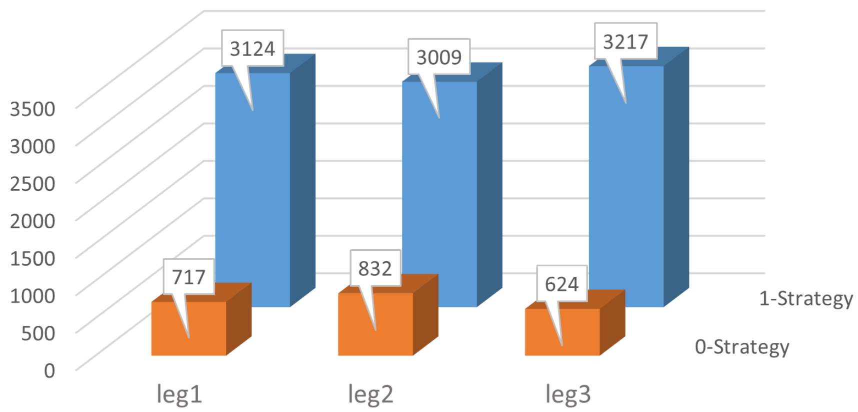

Figure 5.6: Number of times Optimal or Fixed-Strategy utilization.

For the sake of clarity, a table is given showing the percentages of use of the strategies in the three transfers.

Strategy	**leg1**	**leg2**	**leg3**	**total**
0	18.67%	21.66%	16.25%	18.86%
1	81.33%	78.34%	83.75%	81.14%

Table 5.2: Percentages of Optimal or Fixed-Strategy utilization - all sequences.

It can be seen from the results that the percentage of use of the Optimal or Fixed strategy in the first trip does not influence the second and third transfer. The reason is that, as already mentioned above, using Fixed time-strategy does not cost more in terms of ΔV, so the results obtained can be considered with more certainty regarding the choice of strategy for the individual transfer.

Below, graph 5.7 shows the same results but only for the sequences that match those of the original code.

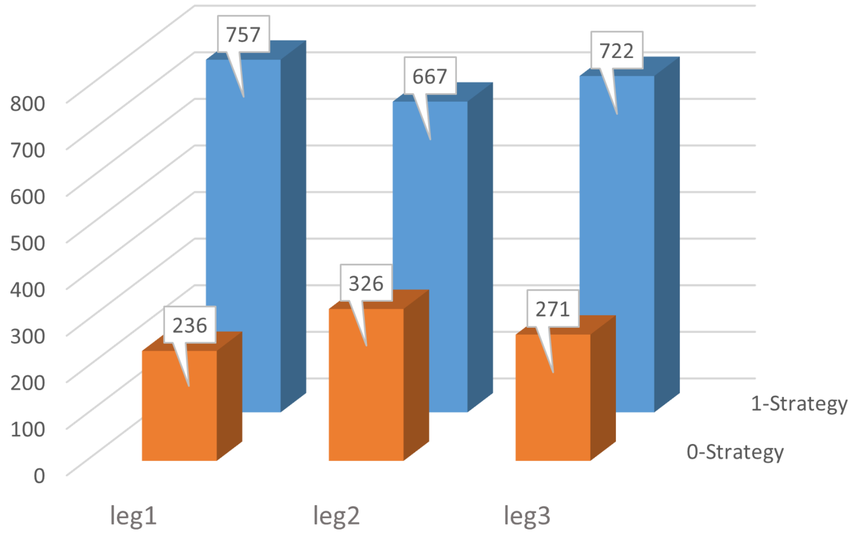

Figure 5.7: Number of times Optimal or Fixed-Strategy utilization.

The table 5.3 shows the same data as graph 5.7 in percentages.

Strategy	leg1	leg2	leg3	total
0	23.77%	32.83%	27.29%	27.96%
1	76.23%	67.17%	72.71%	72.04%

Table 5.3: Percentages of Optimal or Fixed-Strategy utilization - matched sequences.

Again, as can be imagined, the results are similar, only involving fewer sequences and therefore more inaccurate.

Furthermore, after tabulating all the results in excel, as mentioned before, the most critical transfers were selected and compared in terms of ΔV cost with the results of the original code and results obtained from the non-simplified formulation. In table 5.4 are shown all the single transfers that present major errors (critical).

All the critical transfers reported are legs that have never used strategy 0, so the time taken is the maximum 120 days. These 120 days include 30 days of service to apply the de-orbiting kit (10 on each debris apart from the last one) and 30 days for each transfer.

i1	**i2**	ΔV_{thesis}	$\Delta V_{orig.code}$	ΔV_{true}
73	83	0,04822	0,2752	0,082175805
73	57	0,04192	0,23903	0,050853711
80	101	0,05728	0,23154	0,084831331
114	100	0,06387	0,23939	0,092122495
23	101	0,05607	0,21409	0,051783306
23	64	0,06218	0,25475	0,045647532

Table 5.4: Major ΔV errors - single transfers.

The largest and most significant errors, as can be seen, are derived from the original code. At the same time, with regard to the results obtained using the new strategy it can be said that in percentage terms they may be high. Still, numerically speaking, in terms of the difference in ΔV spent, the error is not very large considering the very small values.

In addition, the sequences composed of the four debris with a major error in terms of ΔV were also determined:

i1	**i2**	**i3**	**i4**	ΔV_{thesis}	$\Delta V_{orig.code}$	ΔV_{true}
16	83	73	57	0,23853	0,68739	0,2501441
64	23	101	80	0,14165	0,57321	0,1822622
23	101	80	74	0,19661	0,51327	0,2484318
23	101	80	97	0,11833	0,42382	0,1685173
64	80	101	23	0,15600	0,47937	0,1938680
74	23	101	80	0,34420	0,71603	0,3471131
74	64	23	101	0,30698	0,65305	0,2676678
74	80	101	23	0,25089	0,58776	0,3037299
74	101	23	64	0,29584	0,67739	0,2470956
80	64	23	101	0,15801	0,49187	0,1425001
97	23	101	80	0,24984	0,61139	0,1685173
97	64	23	101	0,21233	0,54478	0,1922324
97	80	101	23	0,15623	0,48056	0,1685173
97	101	23	64	0,20133	0,56940	0,1776828
101	23	64	34	0,34455	0,67711	0,3574506
101	23	64	74	0,25184	0,57813	0,2676678
101	23	64	80	0,15233	0,47262	0,1546842
101	23	64	97	0,17336	0,48742	0,1922324
101	80	64	23	0,14527	0,45753	0,1755481

Table 5.5: Major ΔV errors - full sequence.

Also, in this case, the results obtained with the Fixed time-strategy are much closer to the real value. As already said for the single transfers, the error, if seen in percentage, would seem high, but in terms of numerical difference, the amount is very small and can be considered an acceptable error being a simplified theory.

With regard to critical sequences, as already mentioned, sequences with low ΔV values were selected. The parameter for selection:

- Constraint on $\Delta V \quad \rightarrow \quad \Delta V < 0.2$ km/s

A table summarising the first ten sequences with $\Delta V_{tot} < 0.2$ km/s is then given:

sequence				**strategy**			ΔV_{tot} **[km/s]**		
i1	i2	i3	i4	leg1	leg2	leg3	thesis	other	true
64	101	80	97	1	1	1	0,09046	0,251620	0,143865
23	64	101	80	1	1	1	0,09769	0,374970	0,157610
101	64	80	97	1	1	1	0,10109	0,149860	0,116287
80	101	64	23	1	1	1	0,10351	0,396360	0,157610
23	64	80	97	1	1	1	0,10361	0,244800	0,134804
97	80	101	64	1	1	0	0,10651	0,266100	0,143865
80	101	64	97	1	1	1	0,1158	0,232930	0,206764
97	80	64	101	1	1	0	0,11714	0,164450	0,143865
23	64	101	97	1	1	1	0,11833	0,238110	0,153030
23	101	80	97	1	1	1	0,11833	0,423820	0,168517

It can be seen that, as already mentioned, the results obtained can be considered more precise than those of the original code, but since they are approximations, they are not equal to the real ones. It can be seen from the table that the debris making up the most efficient sequences in terms of ΔV cost are all made up of the same five debris in different positions. Analysing the five debris in question, it was noted that all five have a very similar Ω, clearly also the inclination but this was already known (all debris orbit at an inclination of about 74°).

Chapter 6

Conclusions

The thesis work concerned the implementation in a fortran code of a new strategy that can be exploited to optimize debris removal missions. The mission involves the removal of a sequence of four space debris as efficiently as possible. The Optimal time-strategy, assumes that in a given time, the two debris in question reach $\Delta\Omega$=0, in case of not reaching coplanarity in the predetermined time, the implemented strategy is used, through an initial and a final impulse (which completes the first) leads to the next debris. This strategy allows a simultaneous change of semi-major axis, orbital inclination and longitude of the ascending node.

Since without imposing constraints, too many solutions would have been obtained, as well as the maximum time requirements to reach coplanarity, constraints were also imposed on the ΔV cost ($\Delta V_{tot} < 0.75$ km/s, $\Delta V_{leg} < 0.3$ km/s). A total of 3841 sequences were obtained that met the requirements. Of these possible solutions, only 57, i.e. 1.5%, reached coplanarity using the Optimal time-strategy in all three transfers. As one can imagine, time constraints influenced this result. The costs in terms of ΔV are around 0.5 km/s. It can be noticed that almost all the sequences that are completed with the lowest cost in terms of ΔV instead use Fixed time-strategy, so as can be imagined, they take the maximum expected time (120 days). The costs, in this case, are around 0.1 km/s.

The sequences with results that deviated the most from the original code results were also compared with a non-simplified formulation. It emerged that the results of this work, as far as compared sequences are concerned, are closer to reality. In conclusion, it can be said that the results obtained in this thesis are accurate and close to the non-simplified formulation. They still present some errors that in percentage can seem very big, but they can be considered quite reliable in terms of numerical difference. The results show that exploiting the strategy under consideration in this thesis it is possible to reach the debris that does not reach the coplanarity in a short time even with very low ΔV. This could represent a likely mission scenario in the future, given the need to remove space debris. As mentioned above, one could further improve the results by choosing the best sequences in terms of ΔV_{tot} and t_{tot} and also optimize the distribution of strategies by knowing the debris encounter time a priori.

The first active debris removal mission is planned for 2023 and is part of the ESA's Clean Space project. The mission called 'e.Deorbit' consists of capturing and de-orbiting into the atmosphere of the derelict of the Envisat Earth-observing satellite. This mission will provide an opportunity for European industries to showcase their technological capabilities to a global audience. It will also bring with it the possibility to highlight the problems of future missions.

Bibliography

[1] Anz-Meador, Phillip D. (Jacobs Technology, Inc. Houston, TX, United States) Opiela, John N. (Jacobs Technology, Inc. Houston, TX, United States) Shoots, Debra (Jacobs Technology, Inc. Houston, TX, United States) Liou, J.-C. (NASA Johnson Space Center Houston, TX, United States), "History of On-Orbit Satellite Fragmentations, 15th Edition," 2018.

[2] L. D. . February 2007, "China's Anti-Satellite Test: Worrisome Debris Cloud Circles Earth."

[3] V. authors, "Orbital Debris Qarterly News," *Orbital debris quarterly news*, vol. 13, Issue 2, 2009.

[4] L. D. . March 2013, "Russian Satellite Hit by Debris from Chinese Anti-Satellite Test."

[5] V. authors, "Orbital Debris Qarterly News," *Orbital debris quarterly news*, vol. 20, Issues 1-2, 2016.

[6] N. L. Johnson and D. S. McKnight, *Artificial space debris.* Orbit, a foundation series, Malabar, Fla: Orbit Book Co, 1987.

[7] "Orbital Debris Qarterly News,"

[8] Liou, Jer-Chyi (NASA Johnson Space Center Houston, TX, United States) and Anz-Meador, P. D. (Jacobs Technology Inc. Tullahoma, TN, United States), "An Analysis of Recent Major Breakups in he Low Earth Orbit Region," (Prague), NASA, Jan. 2010.

[9] D. J. Kessler and B. G. Cour-Palais, "Collision frequency of artificial satellites: The creation of a debris belt," *Journal of Geophysical Research: Space Physics*, vol. 83, no. A6, pp. 2637–2646, 1978.

[10] "Space debris by the numbers," Jan. 2021. publisher: ESA.

[11] "HANDBOOK FOR LIMITING ORBITAL DEBRIS," July 2008.

[12] Neal, H. L.; S.L. Coffey; S.H. Knowles, *Maintaining the Space Object Catalog with Special Perturbation*, vol. 97. astrodynamics ed., 1997.

[13] "SSA Programme overview." publisher: European Space Agency.

[14] J. J. Z. J.Sanz Subirana and S. M. Hernández-Pajares, Technical University of Catalonia, "Two-body Problem - Navipedia," 2011.

[15] O. Montenbruck, *Practical ephemeris calculations.* Berlin ; New York:

Springer-Verlag, 1989.

[16] J. Meeus, *Astronomical algorithms.* Richmond, Va: Willmann-Bell, 1st english ed ed., 1991.

[17] United States Naval Observatory, Nautical Almanac Office, Great Britain, Nautical Almanac Office, Great Britain, and Hydrographic Office, *Astronomical almanac for the year 2016: and its companion The astronomical almanac online : data for astronomy, space sciences, geodesy, surveying, navigation and other applications.* 2015. OCLC: 907662321.

[18] M. Courtney and A. Courtney, "The Truth About Ballistic Coefficients," *arXiv:0705.0389 [physics]*, May 2007. arXiv: 0705.0389.

[19] H.-X. Shen and L. Casalino, "Simple ΔV Approximation for Optimization of Debris-to-Debris Transfers," *Journal of Spacecraft and Rockets*, pp. 1–6, Dec. 2020.

[20] D. A. Vallado and W. D. McClain, *Fundamentals of astrodynamics and applications.* No. v. 12 in Space technology library, Dordrecht ; Boston: Kluwer Academic Publishers, 2nd ed ed., 2001.